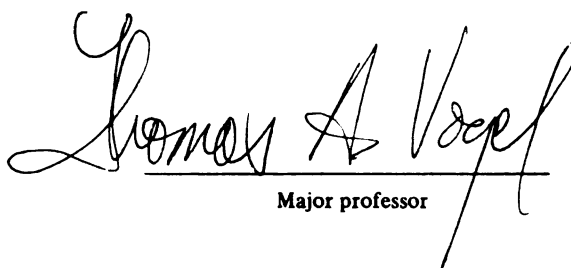This is to certify that the

thesis entitled

A Model for the Origin of the Chemically Zoned
Ammonia Tanks Member of the Timber Mountain Tuff
Due to Crystal Fractionation

presented by

Timothy Patrick Rose

has been accepted towards fulfillment
of the requirements for

Masters degree in _Geology_

Major professor

Date _5/17/88_

A MODEL FOR THE ORIGIN OF THE CHEMICALLY ZONED
AMMONIA TANKS MEMBER OF THE TIMBER MOUNTAIN TUFF
DUE TO CRYSTAL FRACTIONATION

By

Timothy Patrick Rose

A THESIS

Submitted to
Michigan State University
in partial fulfillment of the requirements
for the degree of

MASTER OF SCIENCE

Department of Geological Sciences

1988

ABSTRACT

A MODEL FOR THE ORIGIN OF THE CHEMICALLY ZONED AMMONIA TANKS MEMBER OF THE TIMBER MOUNTAIN TUFF DUE TO CRYSTAL FRACTIONATION

By

Timothy Patrick Rose

The Ammonia Tanks Member of the Timber Mountain Tuff in southern Nevada is a large volume, compositionally zoned ash-flow sheet. Major and trace element chemical analyses of whole, glassy pumice fragments are used to reconstruct the chemical gradients inferred to be present in the pre-eruption chamber. The origin of these compositional trends are shown to be consistent with crystal-liquid fractionation.

The crystal fractionation model predicts that the high-silica rhyolite (78% SiO_2) of the Ammonia Tanks Member can be derived from the quartz latite (59% SiO_2) by fractionating the minerals plagioclase, sanidine, clinopyroxene, biotite and magnetite. However, the common occurence of disequilibrium phenocrysts is not readily explained by this model. Therefore, the possibility that magma mixing acted in conjunction with crystal fractionation is also evaluated. The results of this combined model are consistent with both the chemical data and textural observations.

ACKNOWLEDGEMENTS

TABLE OF CONTENTS

LIST OF TABLES

LIST OF FIGURES

INTRODUCTION

In partially crystallized magma systems, the process
of crystal fractionation is an efficient means of magmatic
differentiation because of the potential it has for
generating liquids of contrasting composition from the
parent liquid (Bowen, 1928). Recent studies have shown that
the evolution of some shallow, silicic magma systems can be
modeled using crystal fractionation as the dominant magmatic
differentiation mechanism (Michael, 1983; Cameron, 1983;
Miller and Middlefehldt, 1984; Wolff and Storey, 1984).

The Ammonia Tanks Member of the Timber Mountain Tuff is
a large volume, compositionally zoned ash-flow sheet in
southern Nye County, Nevada that varies in composition from
a high-silica rhyolite to a quartz latite (Byers, et al.,
1976b). Pumice fragments within a given handsample from
the Ammonia Tanks Member may show as much compositional
variation as that in the entire ash-flow sheet. This
observation can lead to the hypothesis that the rhyolitic
and latitic magmas are genetically related. This
investigation uses chemical and mineralogical data obtained
from individual glassy pumice samples of the Ammonia Tanks
to test the possibility that the high-silica rhyolite was
derived from the quartz latite as a result of crystal
fractionation.

COMPOSITIONAL ZONATIONS IN ASH-FLOW SHEETS

It is generally acknowledged that ash-flow eruptions
result from the rapid, partial evacuation of an upper
crustal magma chamber (Williams, 1941; Smith, 1960).
Ash-flow sheets commonly exhibit stratigraphic variations
in both chemistry and mineralogy (Smith and Bailey, 1966;
Lipman, et al, 1966; Hildreth, 1979). These variations
are inferred to represent an inverted record of the
compositional and thermal zonations that existed in the
magma chamber prior to eruption (cf. Lipman, et al., 1966;
Smith, 1979; Hildreth, 1981; Mahood, 1981; Baker and
McBirney, 1985). Although major element compositional
variations within single ash-flow sheets are often small,
trace element gradients over the same stratigraphic
interval can show a variance of greater than three orders
of magnitude (cf. Hildreth, 1977, 1979; Smith, 1979).
Concomitant with these compositional changes, Fe-Ti oxide
temperatures also change systematically with stratigraphic
height in ash-flow sheets (Lipman, 1971; Hildreth, 1979;
Schuraytz, et al., 1986).

In most eruptive episodes, the bulk chemistry of the
ash-flow sheet shows a trend toward higher temperature,
more mafic, phenocryst-rich compositions with increasing
stratigraphic height. At the same time, the chemical
variation among pumice fragments becomes increasingly
heterogeneous. Schuraytz, et al., (1983, 1986) observed
that the chemical variation among pumice fragments from

2

the top of an ash-flow sheet may be representative of the chemical variation among pumice fragments throughout the entire ash-flow sheet. Based on these observations, it is logical to assume that the most highly differentiated, low temperature, silicic magma is segregated into the roof zone of the magma chamber, and that zoned magma bodies become progressively hotter and more mafic with increasing depth.

Models for the dynamics of magma withdrawal from layered magma reservoirs (Blake, 1981; Spera, 1984; Blake and Ivey, 1986) predict evacuation along subspherical isochrons that tap successively deeper levels in the magma chamber with increasing time. This is consistent with the observed maximum in pumice heterogeneity at the top of the ash-flow sheet since the uppermost part of an ash-flow sheet is believed to represent an instantaneous sampling of magma from all parts of the erupted magma body.

Examination of the compositional and mineralogical variations within pumice fragments from an ash-flow sheet provides the means to reconstruct the variations that existed in the magma chamber prior to eruption. Given this variation, it is then possible to evaluate which magma differentiation processes may have been responsible for the compositional evolution of the magma system. This investigation is directed toward the quantitative evaluation of crystal fractionation as a differentiation mechanism to explain the compositional variations observed

in the Ammonia Tanks ash-flow sheet.

REGIONAL GEOLOGY

The southwestern Nevada volcanic field, in southern Nye County, Nevada was erupted during the late Miocene and early Pliocene, approximately 16 to 9 million years ago (Byers, et al., 1976b). This volcanic field produced at least nine large volume, high-silica ash-flow sheets, numerous smaller rhyolitic tuffs and lava flows, and subordinate amounts of basaltic volcanism, creating an extensive volcanic plateau that once covered an area of more than 11,000 km² (Christiansen, et al., 1977). This activity was contemporaneous with widespread extensional normal faulting that occurred throughout the Great Basin from Eocene to Pliocene time (Lipman, et al., 1966; Christiansen and Lipman, 1972).

A minimum of six calderas have been identified in the southwestern Nevada volcanic field; these are, from oldest to youngest, the Sleeping Butte, Silent Canyon, Claim Canyon, Timber Mountain-Oasis Valley, Black Mountain and Stonewall Mountain calderas (Fig. 1) (Christiansen, et al., 1977). All of these calderas, with the exception of Black Mountain and Stonewall Mountain, are nested together in a tight cluster, possibly indicating a single magmagenetic source (Christiansen, et al., 1977). Recent work by Flood (1987) on the Paintbrush Tuff strongly supports a cyclic evolution model.
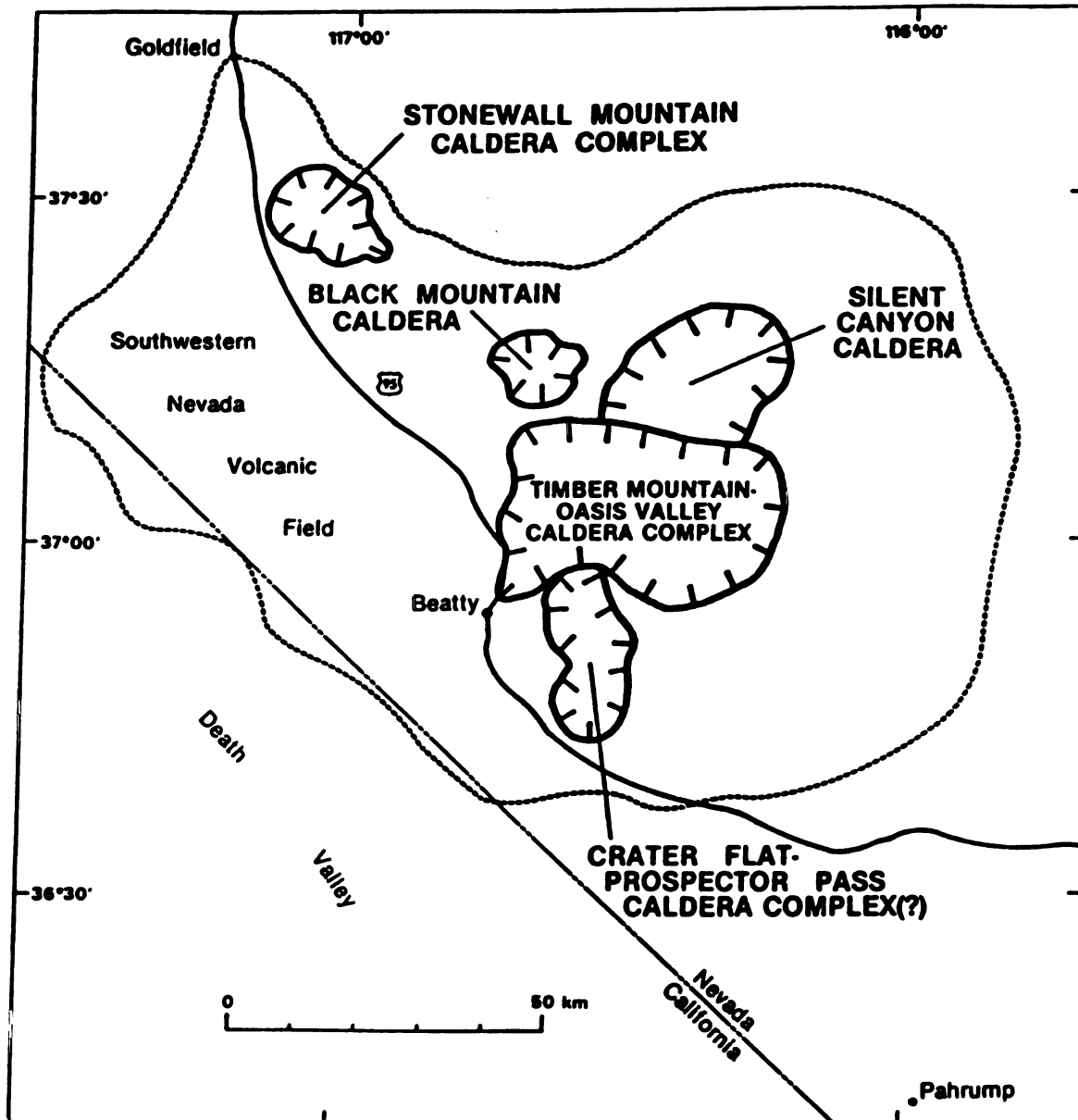
Figure 1. Location of the southwestern Nevada volcanic field, including the Timber Mountain-Oasis Valley caldera complex (after Carr, et al., 1984, and Noble, et al., 1984).

The lower Pliocene, alkali-calcic Timber Mountain Tuff is defined by Byers, et al., (1976b) to include all quartz-bearing ash-flow sheets and all interbedded ash-fall tuff erupted from the Timber Mountain caldera center around 11 million years ago. The tuff includes, in chronological order, the large volume Rainier Mesa and Ammonia Tanks Members, and the intracaldera tuffs of Buttonhook Wash and Crooked Canyon.

Subsidence of the Timber Mountain caldera was initiated by the eruption of the 1200 km³ Rainier Mesa Member of the Timber Mountain Tuff approximately 11.3 million years ago (Christiansen, et al., 1977). This voluminous, compositionally zoned ash-flow sheet consists of an extensive high-silica rhyolite overlain with a partial cooling break by a considerably thinner quartz latitic tuff (Byers, et al., 1976b). Following a hiatus of roughly 0.2 million years, eruption of the 900 km³ Ammonia Tanks Member resulted in further collapse of the Timber Mountain caldera. Twelve separate K-Ar determinations on minerals from the Ammonia Tanks Member yielded an average age of 11.1 million years (Kistler, 1968; Marvin and others, 1970).

The Ammonia Tanks Member is relatively complex in composition as compared with the Rainier Mesa Member, and is probably a composite sheet as defined by Smith (1960). Byers, et al., (1976a) divides the Ammonia Tanks Member into upper and lower cooling units, and these units have been further subdivided by Byers, et al., (1976b) on the

basis of composition into quartz latite and high-silica rhyolite. According to Byers, et al., (1976b), both the upper and lower cooling units are reversely zoned; that is, in both cases, quartz latitic magma was erupted first, followed later by rhyolitic magmas (Byers, et al., 1976b). However, the results of this study show that portions of the Ammonia Tanks ash-flow sheet are normally zoned with respect to composition.

Soon after the Ammonia Tanks eruptions ended, the main cauldron block was uplifted as a resurgent dome. The maximum uplift is at least 1200 m., but this is partially compensated by about 600 m. of displacement along graben faults (Christiansen, et al., 1977).

SAMPLING PROCEDURE

Chemical data used in this study were obtained from the analysis of individual glassy pumice fragments. Glassy samples were used because they are believed to closely represent a discrete parcel of instantaneously quenched magma. That is, with the exception of volatile losses or secondary hydration, glassy pumice fragments (glass + phenocrysts) closely approximate the original composition of the magma. The possibility of chemical modifications due to secondary ground water hydration cannot be ruled out (Aramaki and Lipman, 1965; Lipman, 1965; Noble, 1965, 1967). Pumices fragments that showed evidence of vapor phase alteration, devitrification or intense weathering

were not sampled.

All pumice samples were collected during the summer of 1986. Sampling locations were based on published U.S.G.S. geologic 7 1/2 minute quadrangle maps (Ekrin, et al., 1966; Noble, et al., 1967). The chief sampling criterion was that good stratigraphic control could be maintained. Preferred stratigraphic sections were those that contained contacts with upper or lower stratigraphic units.

Byers, et al., (1976b) observed that the four compositional subunits of the Ammonia Tanks Member (two cooling units, each divided into quartz latitic and rhyolitic components) are not everywhere present outside the area of cauldron subsidence, nor are they precisely correlative over the entire extent of the Ammonia Tanks ash-flow sheet. Although all four units are present on the Timber Mountain resergent dome, field investigations in this area indicated that nearly all of this tuff is devitrified. Therefore none of the stratigraphic sections sampled in this study are representative of all four compositional subunits.

Our sampling focused on obtaining the maximum number of visually different glassy pumice fragments at a given section. Most of the pumice fragments were collected from the non-welded base and top of the sections. In places, entire sections consisted of non-welded tuff. Under these circumstances, samples were collected at equally spaced intervals (usually 10-20 ft.) between the base and the top

of the section. Greatest heterogeneity occurs at the top
of any given section.

Of the 15 sections of Ammonia Tanks collected, three
were selected for sample preparation. The sections used
in the study were selected based on the number of samples
taken, the observed heterogeneity among pumice fragments,
and the stratigraphic control on the section. However,
one of these sections (located at latitude 37° 15'32.5"N,
longitude 116° 20'51.4"W, on the Dead Horse Flat 7 1/2
minute quadrangle map, 0.4 km. N of S. Silent Canyon) was
later eliminated because the mineralogy and trace element
chemistry of samples taken from the section was
significantly different from that of samples taken from the
other two sections. Although the section in question was
mapped as the lower unit of the Ammonia Tanks Member,
because it is chemically similar to the Rainier Mesa Member,
we now believe that it is the Rainier Mesa Member.

ANALYTICAL PROCEDURE

Twenty-seven glassy pumice fragments were analyzed in
this study. Each sample used for analysis was first course
crushed and leached in a solution containing sodium acetate
and glacial acetic acid in order to remove any secondary
carbonate minerals (see Appendix 2 for procedure). The
samples were then powdered by hand in an agate mortar.

For each sample, ten major and twenty trace elements
were determined. Major elements plus Ba, Rb, Sr, Zr, Nb, Y,

Cr, Ni, Cu and Zn were analyzed by a Rigaku X-Ray
fluorescence spectrometer (XRF) at Michigan State University.
XRF analyses were carried out on glass wafers made according
to the procedure described by Hagan (1982) (see Appendix 2).
The remaining trace elements, Sc, Hf, Th, La, Ce, Sm, Eu,
Tb, Yb and Lu were done by instrumental neutron activation
analysis (INAA), also at Michigan State University.
Concentrations were determined by linear least squares
regression on U.S.G.S. standards.

Eight samples representing the entire range of observed
silica content among pumice were selected for detailed
mineralogical analysis. Heavy mineral phenocrysts from a
-60 to +140 sieve size fraction were separated in
tribromomethane (bromoform) and mounted in epoxy, along
with hand picked phenocrysts of quartz, plagioclase,
sanidine, pyroxene, biotite, magnetite and ilmenite. In
addition, thin sections were cut from each of the eight
samples for petrographic and microprobe analyses. All
mineral and glass analyses were made at Lawrence Livermore
National Laboratory using a JEOL 733 electron microprobe.

MAJOR ELEMENT CHEMISTRY

The major element data, reported as weight percent
oxides, is presented in Table 1. Because of secondary
hydration of the glass, all values have been recalculated
to 100 wt%. This allows for comparisons to be made among
samples. Figure 2 illustrates the variation of the major

TABLE 1.   CHEMICAL ANALYSES OF PUMICE FRAGMENTS

SAMPLE ID	AT4-14	AT4-16	AT4-53	AT4-55	AT4-69
WT%					
SiO_2	77.70	65.12	76.75	69.30	77.37
TiO_2	0.14	0.70	0.17	0.37	0.13
Al_2O_3	12.20	17.72	12.55	16.31	12.18
FeO	0.67	2.89	0.74	1.50	0.69
MnO	0.08	0.16	0.07	0.09	0.08
MgO	0.00	0.86	0.00	0.33	0.03
CaO	0.43	2.20	0.42	1.17	0.38
Na_2O	3.76	4.77	3.03	4.62	2.98
K_2O	5.00	5.41	6.24	6.25	6.13
P_2O_5	0.01	0.16	0.01	0.06	0.01
TOTALS	99.99	99.99	99.98	100.00	99.98
PPM					
Zn	37	193	24	40	24
Rb	233	133	201	130	220
Sr	9	382	12	192	10
Y	29	27	28	26	28
Zr	119	697	159	316	125
Nb	41	24	37	27	40
Ba	296	2478	169	852	131
Sc	1.9	7.0	1.3	3.5	1.6
Hf	5.2	15.6	5.7	8.8	5.1
Th	34	17	28	21	33
La	35	200	48	103	32
Ce	69	295	86	172	64
Sm	6.2	7.1	6.6	6.7	6.0
Eu	0.3	3.3	0.4	1.3	0.3
Tb	0.7	0.6	0.6	0.6	0.7
Yb	4.3	2.5	3.7	3.2	3.7
Lu	0.4	0.4	0.4	0.3	0.4

TABLE 1. (Continued)

SAMPLE ID	AT4-75	AT5-2	AT5-3	AT5-4	AT5-8
WT%					
SiO_2	63.77	69.64	77.96	70.66	77.30
TiO_2	0.78	0.44	0.13	0.31	0.16
Al_2O_3	17.56	16.00	12.12	14.88	12.53
FeO	3.28	1.58	0.58	1.30	0.59
MnO	0.12	0.11	0.08	0.09	0.08
MgO	1.67	0.63	0.00	0.94	0.00
CaO	2.62	0.94	0.36	1.83	0.38
Na_2O	4.37	4.28	3.25	3.77	3.35
K_2O	5.48	6.31	5.49	6.14	5.60
P_2O_5	0.34	0.06	0.01	0.08	0.01
TOTALS	99.99	99.99	99.98	100.00	100.00
PPM					
Zn	68	53	66	44	32
Rb	87	138	216	153	219
Sr	491	88	7	179	10
Y	26	28	29	28	30
Zr	801	438	117	295	142
Nb	18	25	32	23	35
Ba	3820	366	74	622	121
Sc	6.9	4.0	1.3	2.7	1.7
Hf	16.7	11.2	4.8	8.9	6.0
Th	14	22	30	22	34
La	151	149	30	90	36
Ce	229	241	59	149	75
Sm	6.9	10.9	5.6	8.2	6.9
Eu	3.4	1.5	0.2	1.0	0.3
Tb	0.6	0.7	0.7	0.8	0.7
Yb	2.5	2.7	2.9	2.7	3.2
Lu	0.3	0.5	0.5	0.5	0.6

TABLE 1. (Continued)

SAMPLE ID	AT5-9	AT5-25	AT5-29	AT5-30	AT5-31
WT%					
SiO_2	70.41	77.46	77.24	65.63	62.85
TiO_2	0.41	0.14	0.15	0.71	0.84
Al_2O_3	15.50	12.47	12.60	17.50	18.06
FeO	1.67	0.65	0.56	2.48	3.72
MnO	0.11	0.08	0.08	0.11	0.12
MgO	0.37	0.02	0.00	0.87	1.51
CaO	1.02	0.38	0.40	1.69	2.94
Na_2O	4.10	3.03	3.33	4.63	4.90
K_2O	6.34	5.77	5.63	6.19	4.71
P_2O_5	0.06	0.01	0.01	0.19	0.33
TOTALS	99.99	100.01	100.00	100.00	99.98
PPM					
Zn	54	29	29	103	125
Rb	140	223	228	96	100
Sr	134	14	10	261	574
Y	28	29	29	27	27
Zr	378	133	128	818	1044
Nb	26	34	35	18	15
Ba	691	90	0	2128	3616
Sc	4.2	1.4	1.5	6.1	6.3
Hf	11.6	5.3	5.0	16.1	19.1
Th	23	32	32	17	13
La	116	35	30	225	148
Ce	196	64	60	383	235
Sm	10.1	5.7	6.1	12.4	10.4
Eu	1.3	0.3	0.2	3.2	3.4
Tb	0.7	0.7	0.7	0.6	0.7
Yb	2.8	2.9	3.0	2.3	2.5
Lu	0.5	0.6	0.5	0.4	0.5

TABLE 1.   (Continued)

SAMPLE ID	AT5-35	AT5-37	AT5-56	AT5-58	AT5-63
WT%					
SiO_2	72.96	77.69	77.67	69.25	62.11
TiO_2	0.29	0.14	0.14	0.39	0.90
Al_2O_3	14.52	12.20	12.21	16.10	18.02
FeO	1.24	0.70	0.56	1.46	3.83
MnO	0.09	0.08	0.06	0.10	0.12
MgO	0.25	0.00	0.00	0.33	1.55
CaO	0.75	0.36	0.31	1.14	3.25
Na_2O	3.70	3.19	3.05	4.29	4.77
K_2O	6.15	5.62	5.99	6.86	5.08
P_2O_5	0.04	0.01	0.00	0.07	0.35
TOTALS	99.99	99.99	99.99	99.99	99.98
PPM					
Zn	42	29	25	38	95
Rb	164	226	214	122	75
Sr	88	8	10	138	615
Y	28	29	29	27	27
Zr	247	132	133	393	1017
Nb	28	32	35	24	12
Ba	394	0	46	709	3990
Sc	2.3	1.7	1.4	3.9	6.9
Hf	8.0	4.8	5.1	11.0	18.9
Th	24	32	32	20	12
La	71	32	32	121	138
Ce	130	60	65	223	228
Sm	8.6	6.0	5.6	10.2	10.3
Eu	0.6	0.2	0.2	1.5	3.5
Tb	0.7	0.7	0.7	0.7	0.7
Yb	2.7	2.9	3.1	2.7	2.4
Lu	0.5	0.5	0.6	0.4	0.4

TABLE 1. (Continued)

SAMPLE ID	AT5-65	AT5-68	AT5-69	AT5-71	AT5-72
WT%					
SiO_2	69.51	73.79	61.31	66.95	64.00
TiO_2	0.45	0.24	1.00	0.56	0.71
Al_2O_3	15.95	14.11	18.00	17.10	18.19
FeO	1.65	1.04	4.43	1.90	3.12
MnO	0.11	0.08	0.13	0.10	0.11
MgO	0.28	0.11	1.75	0.53	1.15
CaO	0.95	0.74	3.40	1.35	2.61
Na_2O	4.24	3.80	4.62	4.41	4.41
K_2O	6.78	6.05	4.96	6.97	5.46
P_2O_5	0.07	0.03	0.40	0.11	0.24
TOTALS	99.99	99.99	100.00	99.98	100.00
PPM					
Zn	46	34	100	47	78
Rb	117	157	72	89	80
Sr	85	83	654	164	524
Y	27	28	26	26	26
Zr	480	220	1154	525	951
Nb	24	30	14	21	14
Ba	499	373	4073	1168	3560
Sc	4.2	1.3	7.3	6.4	6.3
Hf	12.7	7.0	19.6	12.3	17.8
Th	21	23	12	20	13
La	146	53	134	233	135
Ce	265	102	228	393	238
Sm	10.5	6.8	9.9	13.1	9.6
Eu	1.6	0.5	3.4	2.6	3.0
Tb	0.7	0.8	0.7	0.7	0.7
Yb	2.8	2.7	2.4	2.4	2.5
Lu	0.5	0.5	0.4	0.5	0.4

TABLE 1. (Continued)

SAMPLE ID	AT5-75	AT5-79
WT%		
SiO_2	59.44	76.79
TiO_2	1.15	0.13
Al_2O_3	18.23	12.47
FeO	5.05	0.65
MnO	0.13	0.07
MgO	2.24	0.22
CaO	4.21	0.48
Na_2O	4.74	2.81
K_2O	4.33	6.37
P_2O_5	0.49	0.01
TOTALS	100.01	100.00
PPM		
Zn	96	28
Rb	68	214
Sr	819	15
Y	26	29
Zr	1150	127
Nb	10	34
Ba	4703	24
Sc	8.1	1.0
Hf	18.6	4.9
Th	11	31
La	128	30
Ce	217	56
Sm	8.9	5.2
Eu	3.3	0.1
Tb	0.7	0.8
Yb	2.4	3.0
Lu	0.3	0.5

NOTE: All major element analyses
       have been normalized to 100%
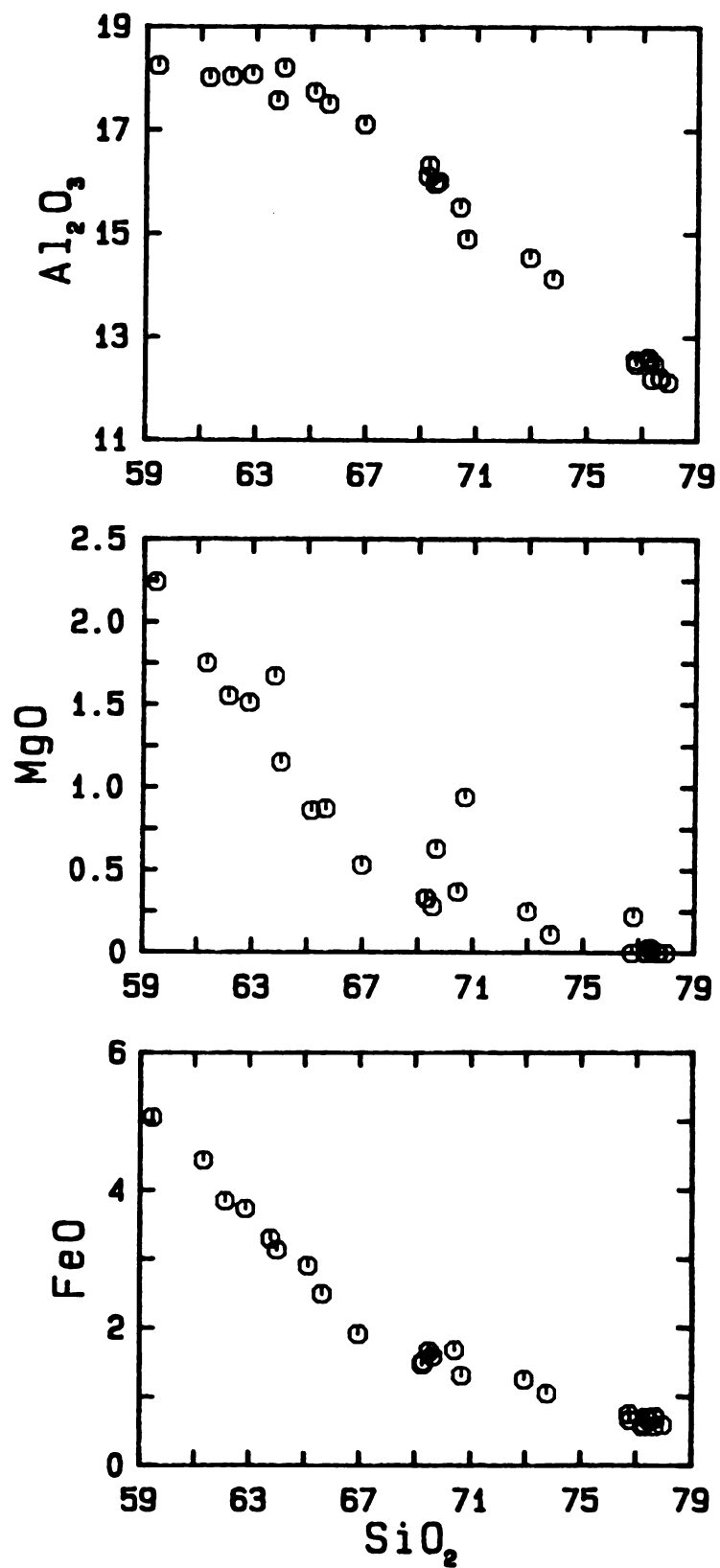
Figure 2. Variation of major element oxides versus silica.
Units in weight percent.
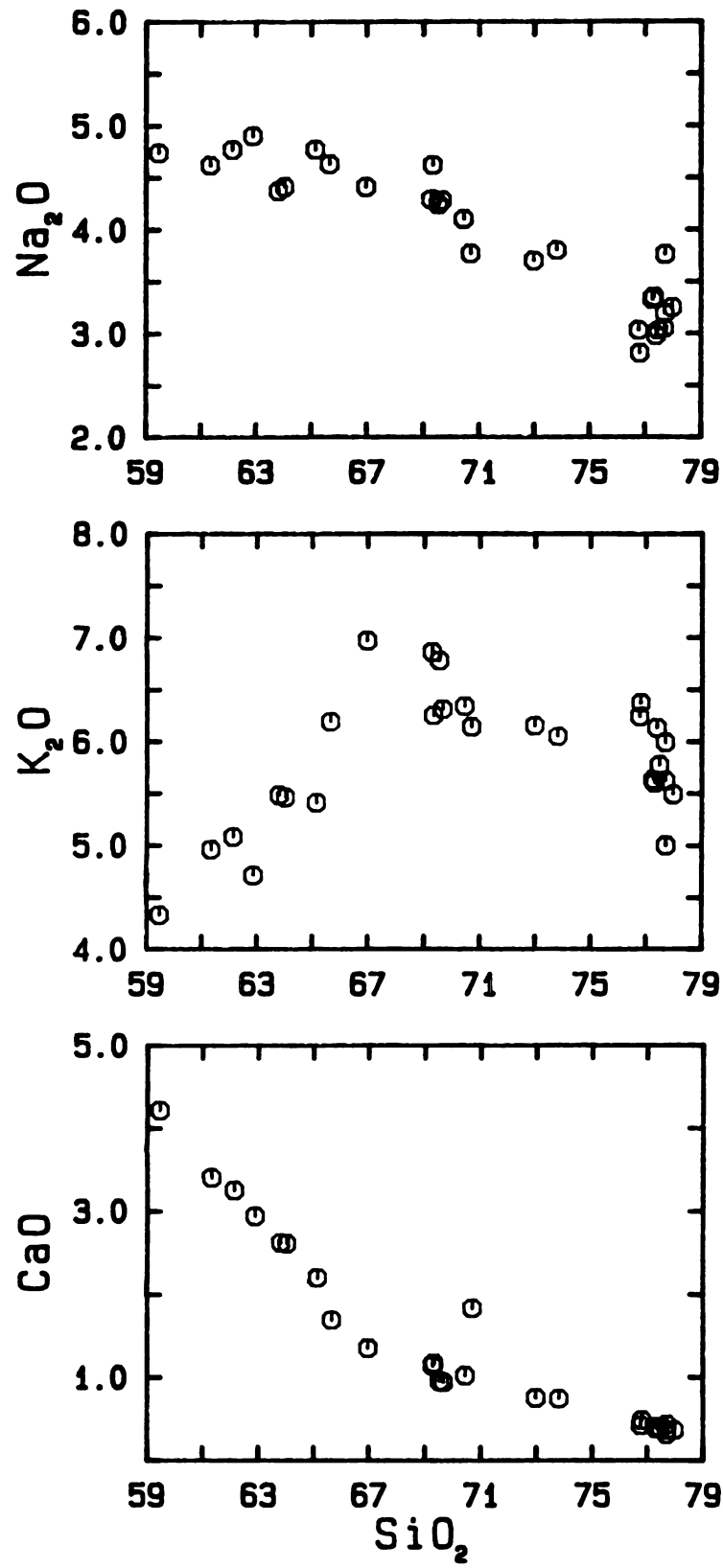
Figure 2. (continued) Variation of major element oxides versus silica. Units in weight percent.
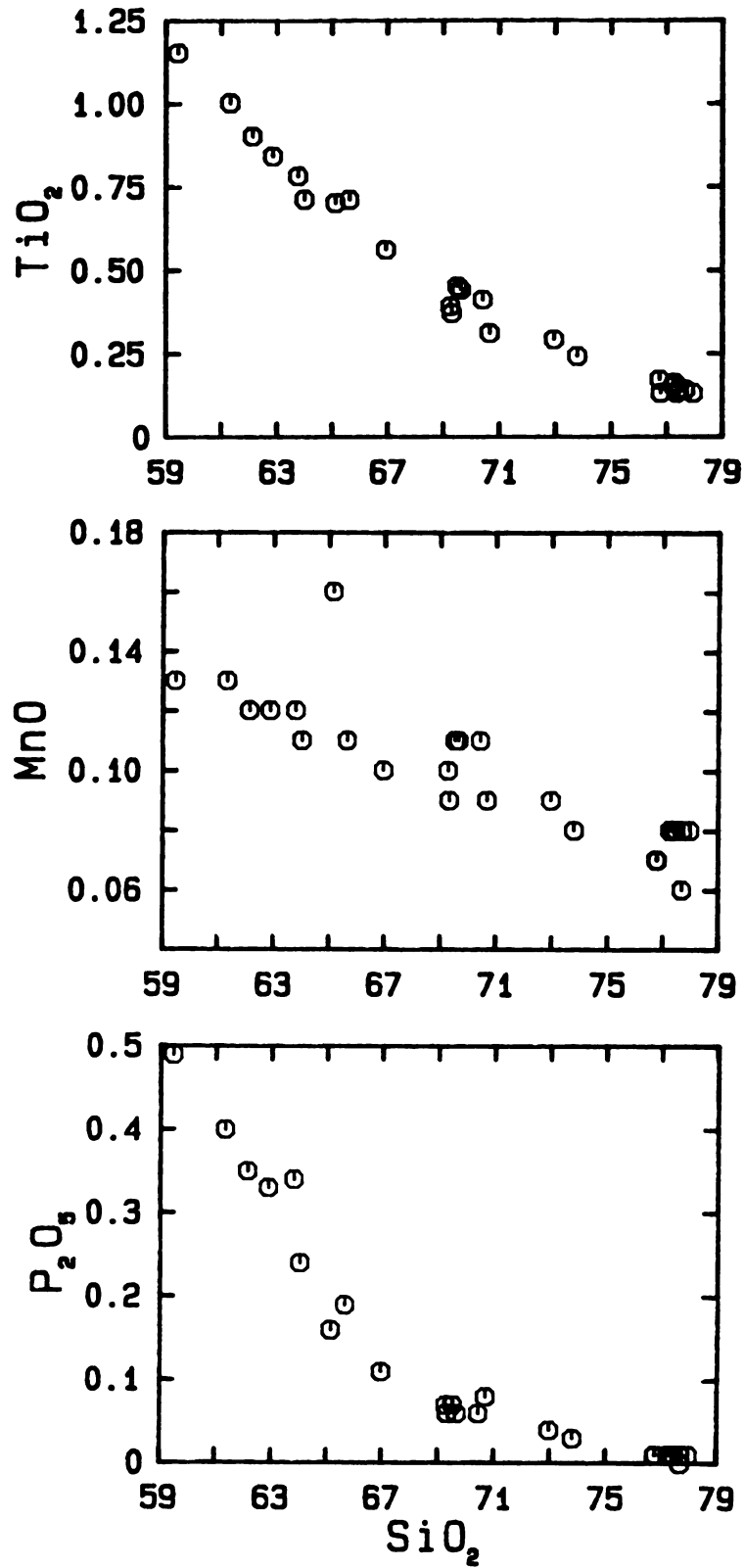
Figure 2. (continued) Variation of major element oxides versus silica. Units in weight percent.

elements plotted against silica. Major element oxide
variation diagrams provide a guide to identifying where
various crystal phases may have been fractionating from the
melt. Inflections in the chemical trends represented on
these diagrams may indicate that a mineral phase had begun
to crystallize at that composition. SiO_2 was chosen as
the abscissa on these diagrams because of it's large
compositional range. Furthermore, silica has a non-
overlapping range of values for many of the minerals used
in the fractionation model. This makes it easier to
identify specific mineral control on any of the individual
variation diagrams because different minerals will not plot
at the same point (Wright, 1974).

Most of the major element variation diagrams, with the
exception of Na_2O and K_2O, exhibit curvilinear trends with
little scatter. Scatter on the Na_2O and K_2O diagrams may
indicate secondary hydration processes. Well defined
changes in slope occur in the Al_2O_3, FeO, MgO, CaO, K_2O
and P_2O_5 plots v.s. SiO_2, possibly indicating the
fractionation of minerals containing these elements as
important constituents.

The twenty-seven glassy whole pumice fragments analyzed
in this study exhibit a range in SiO_2 from 59.4 wt% to
78 wt%. Previous whole rock analyses of the Ammonia Tanks
Member are reported to range from 66 wt% to 77 wt% (Byers,
et al., 1976b). Silica gaps appear between 67% and 69.25%
SiO_2, between 70.7% and 73% SiO_2, and again between 73.8%

and 76.8% SiO_2. It may be that these discrete compositional breaks indicate the presence of sharp compositional interfaces that existed in the magma chamber prior to eruption. On the other hand, it is possible that some or all of the apparent compositional gaps reflect sampling bias.

The variation of major elements with stratigraphic height for the sampling locations used in this study is well illustrated by the Pahute Mesa Road Section #5 (see Appendix 1 for location). Twenty-one of the twenty-seven glassy pumice fragments analyzed were taken from this section. At the base of the section, pumice compositions range from 78 wt% to 69.6 wt% SiO_2, whereas approximately 30 ft. above the base, the range is 77.7 wt% to 62.8 wt% SiO_2. At the top of the section, roughly 100 ft. above the base, pumice compositions vary from 77.7 wt% to 59.4 wt% SiO_2. Mafic pumice fragments become increasingly abundant higher in the section, whereas high-silica rhyolite pumice fragments are ubiquitous throughout. Similar trends were observed among glassy pumice fragments taken from the other stratigraphic section used in this study. These observations indicate that the portions of the Ammonia Tanks ash-flow sheet used in this study are normally zoned with respect to composition.

TRACE ELEMENT CHEMISTRY

Whereas major element concentrations in ash-flow sheets typically exhibit less than one order of magnitude in variation, trace element variations can exceed three orders of magnitude (Hildreth, 1979). Magma differentiation mechanisms are known to have a large effect on the distribution of trace elements in a magma chamber. The careful evaluation of trace element distributions in eruptive sequences may be used to infer which magma differentiation processes may have been operating in the magma chamber.

Trace element concentrations for samples analyzed in this study are presented in Table 1. Figure 3 shows element enrichment factor diagrams, similar to those used by Hildreth (1979) except that points are plotted rather than vertical bars (see Wolff and Storey, 1984). Each point represents the ratio of element concentrations in two different pumice fragments. In each case, the numerator represents the sample that is more highly evolved with respect to silica. It is inferred that these higher silica samples represent magma that was erupted from the highly fractionated top of the magma chamber (Hildreth, 1979; Smith, 1979). This inference is supported by the observed enrichment of incompatible elements and depletion of compatible elements in high silica samples.

Figure 3a is a plot of the concentrations of seventeen minor and trace elements in the most silicic pumice

22
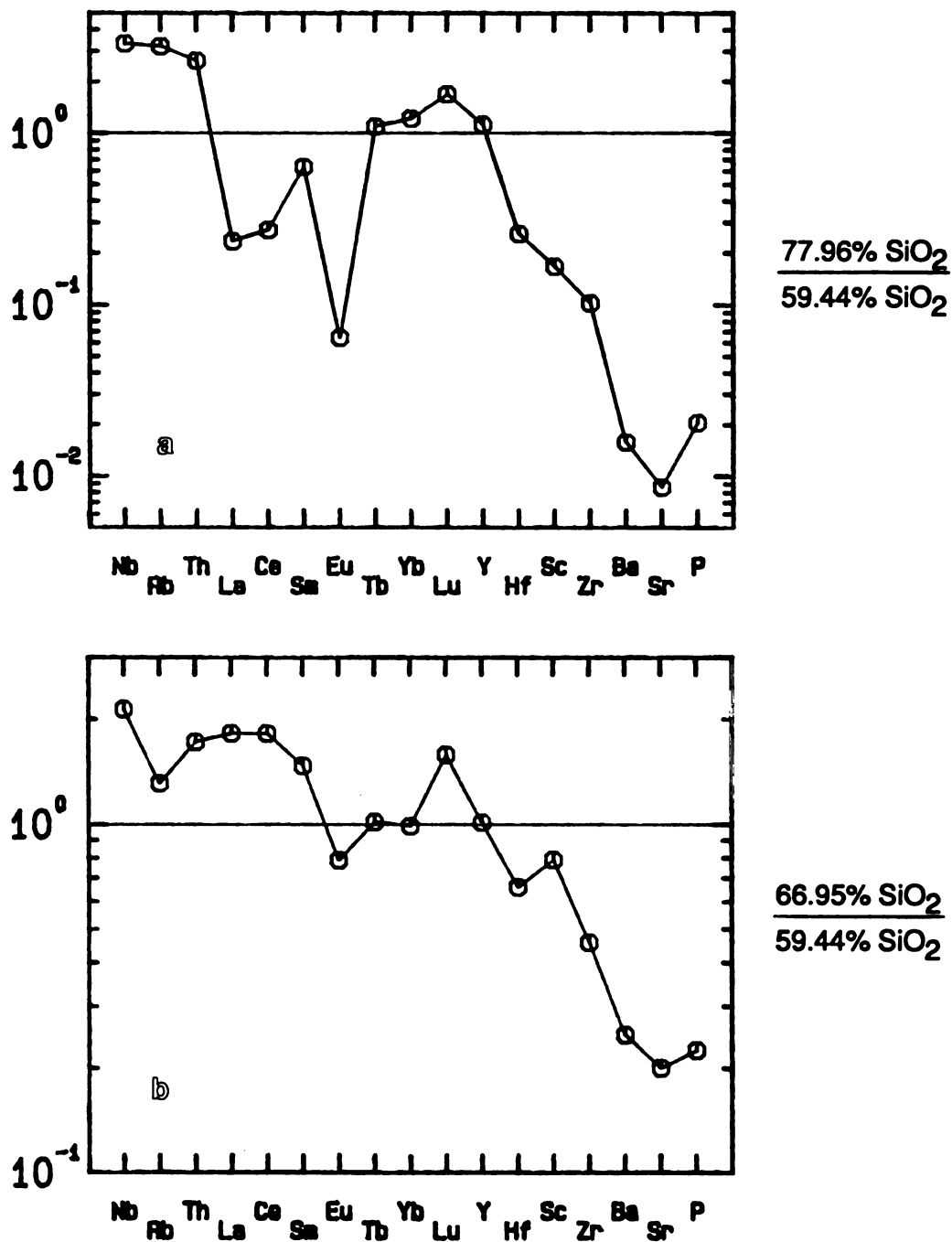
Figure 3. Enrichment factors for 17 minor and trace elements.
(a) Element concentrations in the most silicic pumice fragment
divided by concentrations in the most mafic pumice fragment.
(b) Element concentrations in a pumice fragment of intermediate
silica composition divided by concentrations in the most mafic
pumice fragment.

fragment (AT5-3; 77.96% SiO_2) divided by their
concentrations in the most mafic pumice fragment (AT5-75;
59.44% SiO_2). The elements are arranged along the x-axis
according to the following scheme (from left to right):
highly incompatible trace elements (Nb, Rb, Th), REEs
(including Y because of its similar behavior), compatible
trace elements, in order of increasing compatibility in
the high silica pumice (Hf, Sc, Zr, Ba, Sr), and lastly,
P (to illustrate the control of apatite fractionation).
It can be seen that Ba, Sr, P and Eu are highly
depleted in the silicic sample, while Rb, Nb and Th are
markedly enriched in this sample. The HREEs and Y are
also enriched in the silicic sample, but the LREEs
become progressively less enriched in the silicic
sample as atomic number decreases. Sc, Hf and Zr are
more enriched in the mafic sample.

Figure 3b is a plot of the ratio of element
concentrations in a pumice fragment of intermediate
silica composition (AT5-71; 66.95% SiO_2) divided by the
concentrations in the most mafic pumice fragment (AT5-75).
A number of differences between this plot and the plot
just described (figure 3a) are apparent. One important
distinction is the behavior of the LREEs. La, Ce and Sm
all exhibit incompatible trends in figure 3b, but
compatible trends in figure 3a. This tendency toward
increased compatibility of the LREEs in higher silica
samples can be accounted for by the fractionation of a

LREE-bearing phase (see discussion below). Similarly,
the increasing compatibility of Eu, Hf, Zr, Ba, Sr and P
in figure 3a relative to figure 3b is attributable to
crystal fractionation of plagioclase (Eu,Sr), sanidine
(Ba,Sr), zircon (Hf,Zr) and apatite (P). Strongly
incompatible elements such as Nb, Rb and Th are more
enriched in high-silica samples (figure 3a) than in
those of intermediate silica compositions (figure 3b).

   Figure 4 illustrates the chemical variation of
selected REE's for all analyses of the Ammonia Tanks
Member. The ordinate values represent the ratio of the
elemental concentration in the sample to the average
concentration of that element in chondrites given by
Haskin, et al., (1968). Although most of the elements
show a fairly continuous distribution in composition,
three compositional groups can be distinguished for the
element europium. The well defined uppermost group (n=9)
consists of mafic samples containing <67% SiO_2, and >2.5
ppm Eu. Samples in the middle group (n=6) were found
to contain between 69% and 70.6% SiO_2 and 1-2 ppm Eu
while those in the lowermost group (n=12) contain >73%
SiO_2 and <0.7% Eu. (The compositional break between
the middle and lower groups occurs at a normalized
concentration of about 10). It is notable that both of
the compositional breaks on the REE plot coincide with
silica gaps that were noted in the major element
chemistry discussion. The large negative Eu anomaly
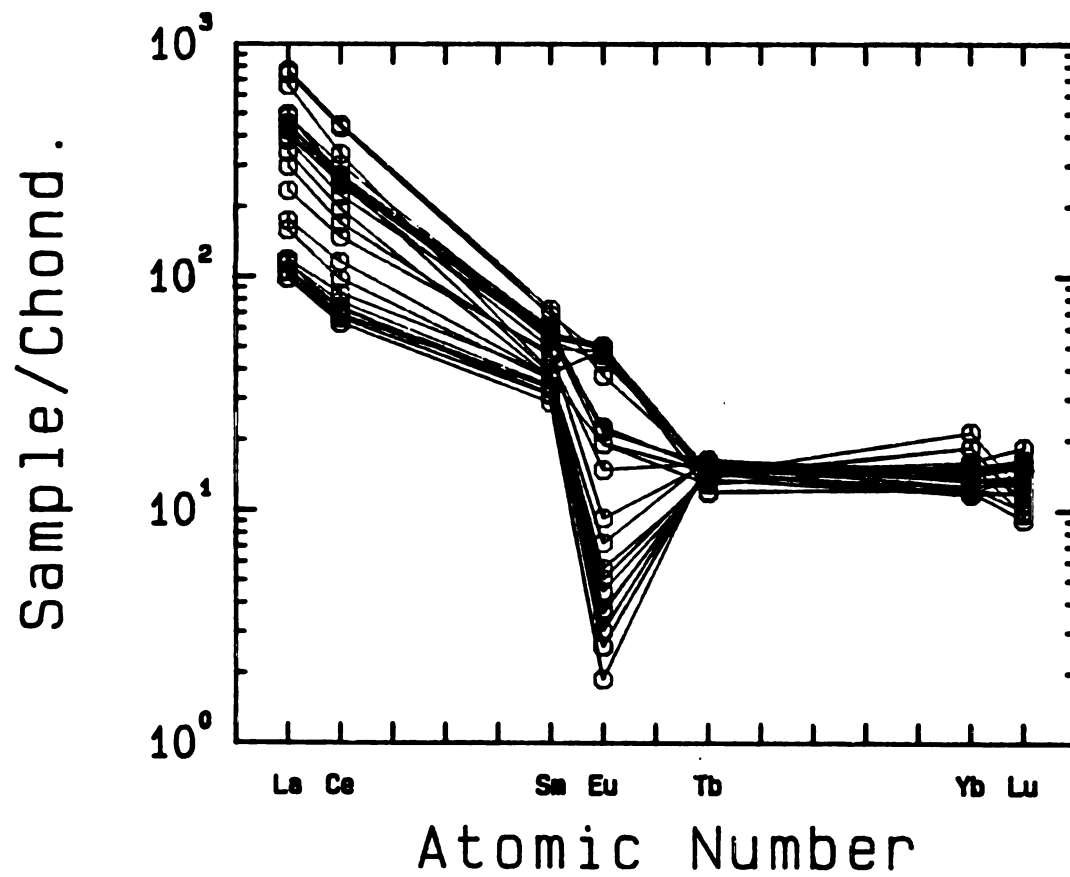
Figure 4. Chondrite-normalized REE abundances (log scale) versus atomic number.

seen in the high-silica rhyolite probably reflects the
fractionation of plagioclase.

In figure 5, various trace elements are plotted against
SiO_2. The elements Ba, Zr, Sr, Sc and Eu all decrease
with increasing SiO_2. These trends are consistent with
crystal fractionation of plagioclase, sanidine,
clinopyroxene and zircon. Conversely, Rb, Nb and Th
behave as incompatible elements, increasing with SiO_2.
Ce behaves incompatibly up until 67% SiO_2, after which
it drops off rapidly in concentration. This behavior is
best explained by the observation that the LREE-bearing
phase chevkinite is present in all samples containing >67%
SiO_2. La exhibits behavior identical to Ce. The leveling
off of the Ce trend above 71% SiO_2 may indicate a decrease
in chevkinite fractionation, or it may indicate another
phase (opx?) was actively partitioning the LREE's between
69% and 71% SiO_2.

Inflections in the Ba, Sr and Al_2O_3 trends at around
65% SiO_2 probably mark the initiation of sanidine
fractionation. More significantly, the inflections at 67%
SiO_2 on the Ba, Zr, Rb, Sr, Sc and Eu plots are coincident
with inflections seen on major element plots of FeO, MgO,
CaO, K_2O and P_2O_5 v.s. SiO_2. These inflections may be
related to the fractionation of mineral phases, or they
may indicate the presence of a compositional discontinuity
in the magma chamber associated with the silica gap
observed between 67% and 69% SiO_2. Well defined changes
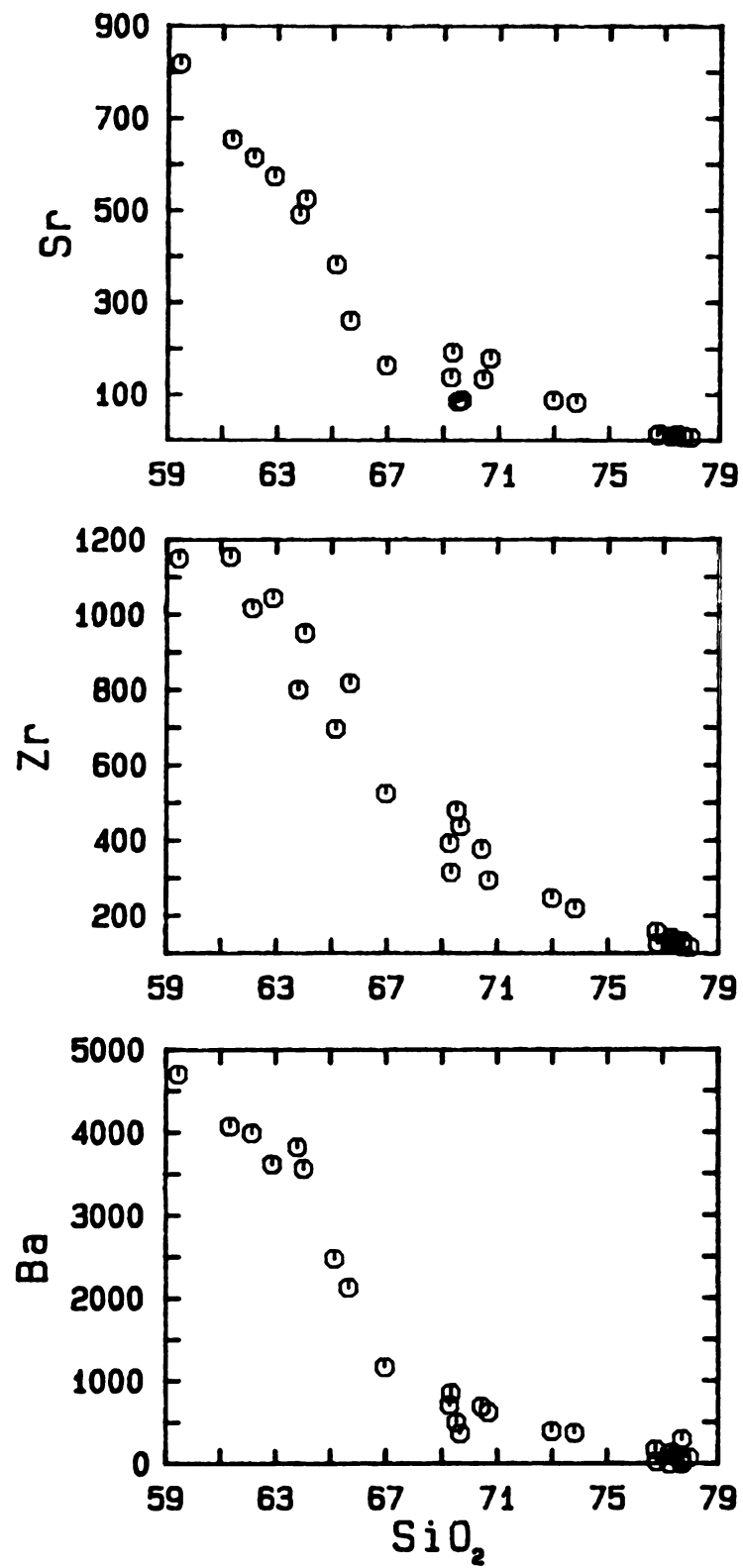
Figure 5. Variation of trace element abundances (ppm) versus silica (wt %)
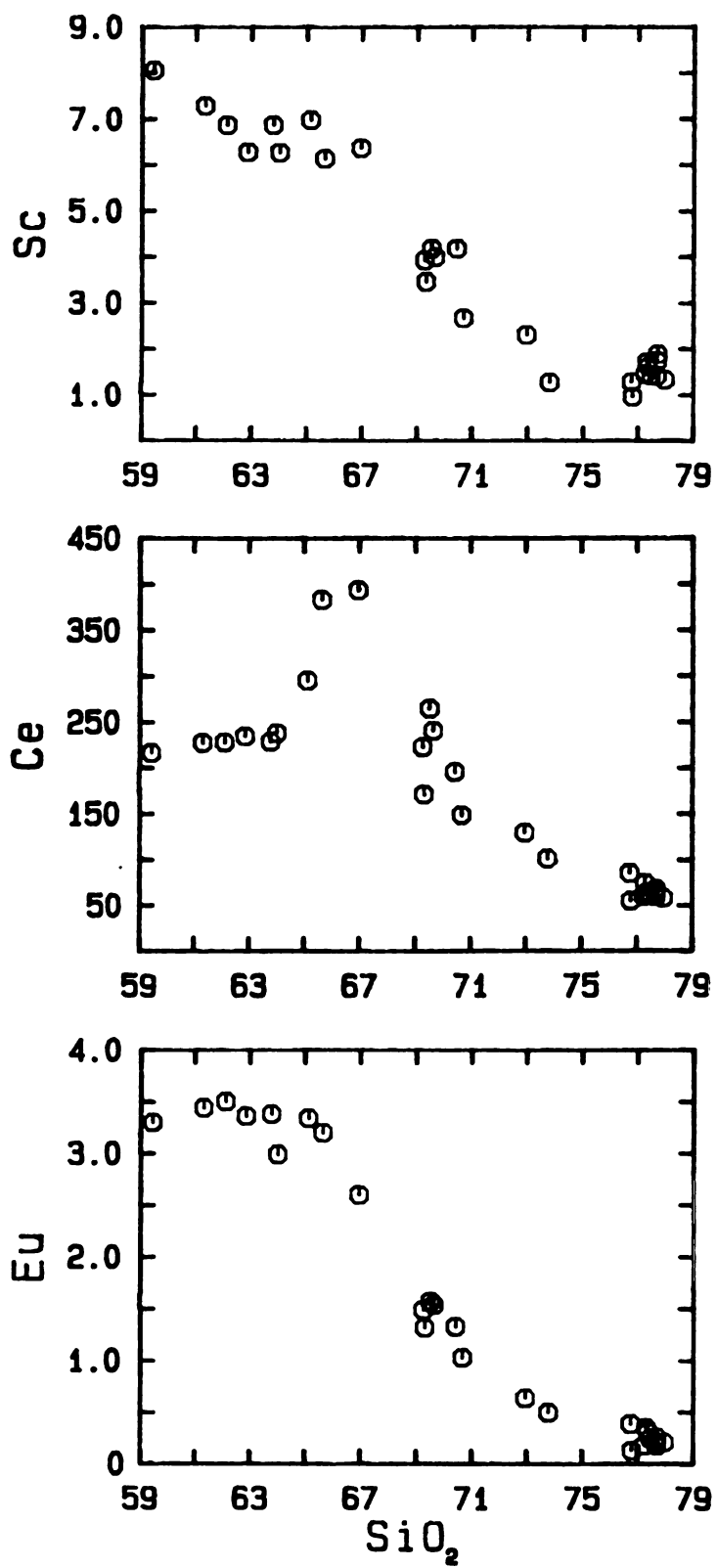
Figure 5. (Continued) Variation of trace element abundances (ppm) versus silica (wt %)
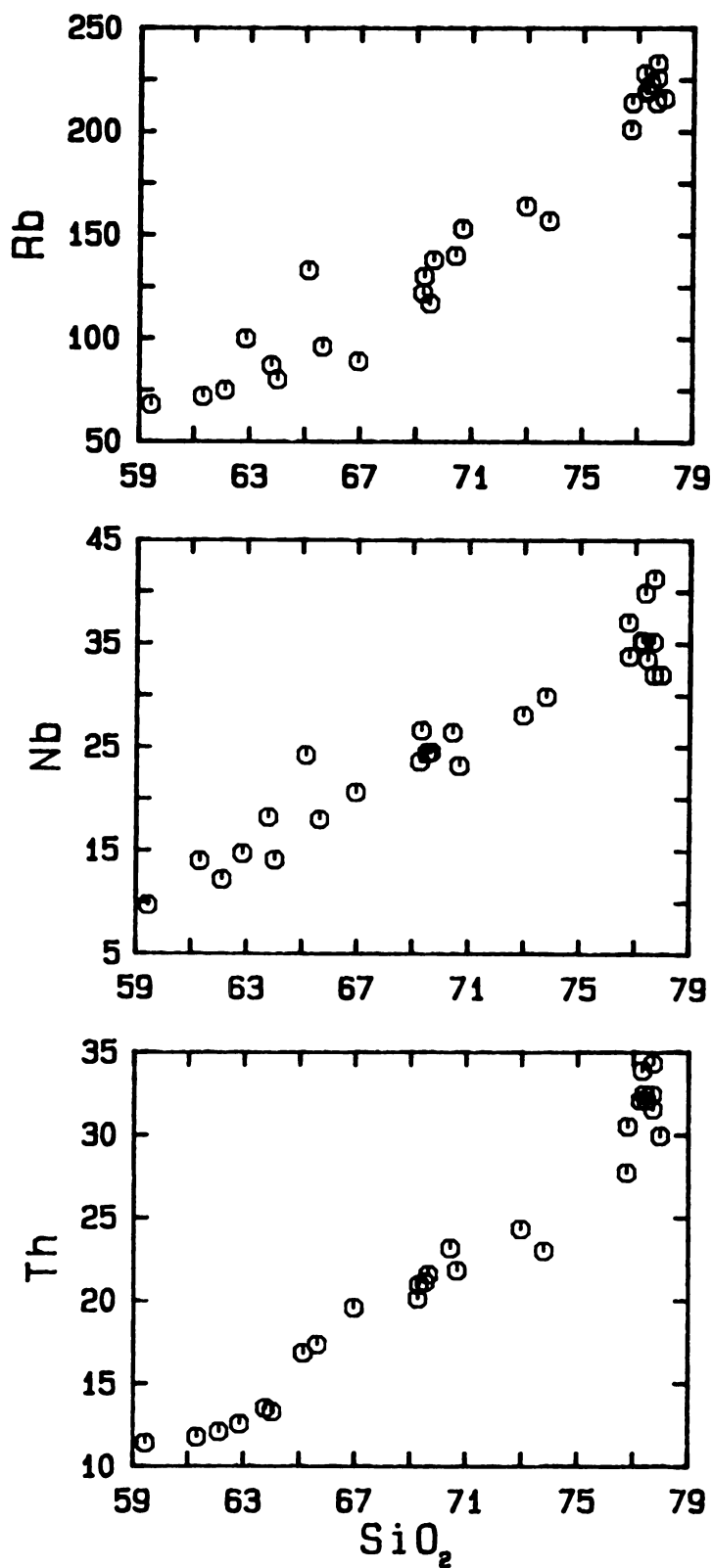
Figure 5. (Continued) Variation of trace element abundances (ppm) versus silica (wt %)

in slope also occur on the incompatible trace element plots (Rb, Nb, and Th) for SiO_2 compositions >76%. These inflections correspond to the gap in silica composition that occurs between roughly 73.8% and 76.8% SiO_2, possibly indicating the presence of a compositional discontinuity at a high level in the magma chamber.

MINERALOGY

Brief discussions of the variations in the chemistry of phenocrysts in whole rock samples of the Timber Mountain Tuff are given by Byers, et al., (1976b) and Broxton, et al., (1985). The mineralogy of only glassy pumice samples will be discussed here. Representative major element analyses of phenocrysts from eight glassy pumice samples are presented in Table 2. All mineral analyses were made at Lawrence Livermore National Laboratory using a JEOL 733 electron microprobe. Systematic variations in phenocryst assemblages, chemistry and modal percentages are observed in Ammonia Tanks pumice fragments as SiO_2 increases, reflecting the overall compositional evolution of the magma chamber.

Plagioclase phenocrysts from 0.5 to 4 mm long occur in all glassy pumice samples and are the dominant mineral phase in samples containing <67% SiO_2. They are typically euhedral to subhedral and commonly exhibit resorption textures, particularly in samples containing <69% SiO_2. Many of the phenocrysts are broken. Plagioclase becomes

TABLE 2.   REPRESENTATIVE MINERAL ANALYSES

(Weight percent oxides)

PLAGIOCLASE

Sample	AT5-35	AT5-69	AT5-63	AT5-69	AT5-75
Mineral ID	27	48	39	50	91
SiO_2	63.95	58.75	58.11	54.20	49.10
Al_2O_3	22.59	24.34	26.09	29.03	32.91
FeO	0.26	1.12	0.37	0.42	0.29
MgO	0.00	0.00	0.01	0.04	0.03
CaO	2.77	5.02	7.07	9.78	14.47
Na_2O	8.71	7.57	6.67	5.63	2.90
K_2O	1.72	1.86	1.25	0.61	0.19
BaO	0.00	0.30	0.32	0.19	0.00
TOTALS	100.00	98.96	99.89	99.90	99.89

SANIDINE   KNEBELITE

Sample	AT5-35	AT5-71	AT5-71	AT5-3	AT5-3
Mineral ID	28	64	63	04	05
SiO_2	65.48	64.08	63.38	30.93	30.63
Al_2O_3	19.29	20.37	21.62	0.00	0.04
FeO	0.09	0.25	0.35	49.13	45.44
MgO	0.00	0.00	0.00	0.00	0.00
CaO	0.38	0.90	2.49	0.02	0.10
Na_2O	5.16	5.78	7.66	0.00	0.03
K_2O	9.33	8.19	4.35	0.00	0.02
BaO	0.25	0.26	0.07	0.04	0.03
TiO_2				0.00	0.10
MnO				19.86	23.60
NiO				0.02	0.01
TOTALS	99.98	99.83	99.92	100.00	100.00

TABLE 2.   (Continued)

		BIOTITE		HORNBLENDE
Sample	AT5-3	AT5-35	AT5-72	AT5-75
Mineral ID	03	25	74	90
SiO_2	41.96	40.58	37.23	42.33
Al_2O_3	13.12	13.67	15.67	11.73
FeO	12.73	15.06	14.05	11.67
MgO	18.90	16.56	14.92	14.40
CaO	0.19	0.28	0.01	11.64
Na_2O	0.41	0.58	0.75	2.63
K_2O	8.55	8.00	7.47	1.21
TiO_2	3.19	4.59	6.99	3.99
MnO	0.90	0.43	0.28	0.36
P_2O_5	0.00	0.00	0.00	0.00
BaO	0.04	0.24	2.63	0.05
NiO	0.00	0.00	0.00	0.00
TOTALS	99.99	99.99	100.00	100.01

		CLINOPYROXENE		ORTHOPYROXENE
Sample	AT5-58	AT5-71	AT5-75	AT5-58
Mineral ID	10	58	86	13
SiO_2	52.66	52.66	51.86	52.56
Al_2O_3	1.18	1.47	2.14	0.76
FeO	9.08	9.21	7.94	18.90
MgO	12.69	13.72	15.90	23.83
CaO	21.12	20.18	20.31	1.18
Na_2O	0.69	0.73	0.65	0.05
K_2O	0.02	0.00	0.00	0.02
TiO_2	0.20	0.39	0.47	0.19
MnO	1.91	1.54	0.69	2.31
P_2O_5	0.00	0.00	0.00	0.00
BaO	0.44	0.08	0.04	0.00
NiO	0.00	0.02	0.00	0.20
TOTALS	99.99	100.00	100.00	100.00

TABLE 2.   (Continued)

MAGNETITE

Sample	AT5-3	AT5-58	AT5-63	AT5-72
Mineral ID	08	31	42	82
Cr_2O_3	0.03	0.05	0.00	0.06
Al_2O_3	0.64	1.45	2.85	1.98
MgO	0.71	1.42	3.76	2.30
FeO	90.57	85.03	80.58	74.30
TiO_2	4.92	8.98	11.81	20.03
MnO	3.12	3.07	1.01	1.31
TOTALS	99.99	100.00	100.01	99.98

ILMENITE

Sample	AT5-3	AT5-35
Mineral ID	09	21
Cr_2O_3	0.00	0.00
Al_2O_3	0.06	0.00
MgO	1.56	1.64
FeO	44.77	51.94
TiO_2	46.91	43.05
MnO	6.71	3.36
TOTALS	100.01	99.99

NOTE: All analyses have been normalized to 100%

progressively more sodic with increasing silica content. The mole fraction of anorthite varies between An_{13} and An_{38} in the rhyolite and high-silica rhyolite, whereas in the quartz latite the variation is from An_{21} to An_{72}. The average plagioclase composition is around An_{33}. Zoned crystals with more calcium-rich cores are common, particularly at whole pumice compositions below 69% SiO_2.

Sanidine first appears in samples containing 61% SiO_2, and is the predominant phenocryst phase in samples with >67% SiO_2. Sanidine crystals are euhedral to subhedral, ranging in size from 0.5 to 4 mm. Resorption textures and fracturing are common, but less prominent than in plagioclase. The compositional variability throughout the ash-flow sheet is small, ranging from Or_{46} to Or_{54}, with a variation in the celsian mole fraction ranging from Cn_0 to Cn_4. Sodic overgrowths on more calcium-rich plagioclase cores may contain up to 24 mole percent Or. Quartz occurs only in the high-silica rhyolite, where it is fairly abundant as euhedral phenocrysts ranging from 2 to 4 mm in length. Resorption textures were not noted, but some grains are fractured.

Magnetite is present in all samples, ranging from 0.1-0.5 mm euhedral grains in the rhyolite and high-silica rhyolite, to large clumps of subhedral grains up to 1 mm in size in the quartz latite. Ilmenite is at least an order of magnitude less abundant than magnetite. In the quartz latite, magnetite and ilmenite often occur with, and are

included in the ferromagnesium minerals, particularly
pyroxenes. In contrast, the ilmenite and magnetite in the
more rhyolitic samples occur in smaller, more isolated
groups of grains, or individually, often associated with
zircon, chevkinite and apatite. Magnetite and ilmenite are
increasingly enriched in MnO with increasing silica.

Biotite is the most abundant ferromagnesium silicate in
all samples, occuring as euhedral, 0.5 to 3 mm phenocrysts.
It contains up to 3.5% BaO in the more mafic samples, and
becomes progressively more enriched in MgO with increasing
SiO_2. MgO/MgO+FeO in biotite varies from 0.52 to 0.60.

Clinopyroxene is found in all samples examined containing
<73% SiO_2. It occurs as blocky, euhedral to subhedral
phenocrysts, generally <1 mm in length. Mg-rich
orthopyroxene is found in pumice samples containing between
69% and 73% SiO_2. It is found associated with opaque
oxides and trace phases, typically as euhedral, yellowish-
green prismatic crystals, 1 mm or less in size.
Orthopyroxene compositions range from En_{67} to En_{68}, and
clinopyroxene ranges from $Wo_{39}En_{53}Fs_8$ to $Wo_{44}En_{42}Fs_{14}$.
Many clinopyroxene crystals are slightly zoned, typically
with more Mg-rich cores and Fe-rich edges. Trace amounts
of hornblende occur in sample AT5-75 (59.44% SiO_2) as 1 mm
partially resorbed crystals intergrown with plagioclase.
They are not believed to be cognate to the Ammonia Tanks.

Trace amounts of the minerals apatite, zircon, sphene,
chevkinite and knebelite are also found in the Ammonia Tanks

ash-flow sheet. Apatite is most abundant in the quartz latite occuring a stubby, six-sided euhedral crystals up to 0.5 mm in size. It is often found as poikilitic grains in silicate phases. Apatite gradually becomes smaller and more acicular as the whole pumice silica composition increases. Zircon is present in all thin sections as 0.1 mm, euhedral crystals. Zircon tends to occur in biotite phenocrysts in the quartz latite, but is more often associated with magnetite and chevkinite in rhyolitic samples. Sphene is found only in the high-silica rhyolite as small (<1 mm), isolated, wedge-shaped crystals. Chevkinite, a LREE-rich silicate mineral, is present in all samples examined containing >67% SiO_2. It occurs as dark reddish-brown, subequant grains up to 0.1 mm in size, associated with the opaque Fe-Ti oxides. Knebelite, the Mn-rich analogue of fayalite, occurs as minute, needle-like crystals in the high-silica rhyolite. Knebelite normally occurs in rocks associated with Fe-Mn ore deposits or their metamorphic equivalents (Deer, et al., 1962). To the author's knowledge, this is the first reported occurence of this mineral in ash-flow sheets.

EVALUATION OF CRYSTAL FRACTIONATION

Crystal fractionation can be quantitatively evaluated using two types of tests. Major element multiple linear regressions are used to determine the percentages of mineral phases that must be fractionated from the parent

magma to produce the derivitive magma. Trace element
data is then used to test the validity of the major
element regression. Maximum and minimum mineral/liquid
distribution coefficients (K_D values) are used to
calculate a predicted range of trace element
concentrations in the derivitive liquid based on the
amount of crystal fractionation predicted by the major
element regression. If the model is valid, then the
trace element concentrations observed in the derivitive
magma should fall within the predicted range.

The major element multiple linear regressions were
initiated by choosing the least evolved pumice sample
(AT5-75, 59.44% SiO_2) and regressing it against a
slightly more evolved sample (AT5-63, 62.11% SiO_2) plus
all potential combinations of major phenocryst phases.
If individual phase chemistries showed a range in
composition, then more than one composition was tested
in the regression. Once a reasonable regression model
was determined for the first step, then the former
derivitive magma (AT5-63 in step 1) became the new parent
magma, and the process was repeated with a new, more
silicic derivitive magma.

A total of six major element multiple linear
regressions were used to model the entire compositional
evolution exhibited by Ammonia Tanks pumice fragments
(see Table 3). In general, the best fit model with the
smallest sum of the squares of the residuals was chosen

for each step. One exception was made with the first
step in the regression analysis. The model for step 1
that had the lowest residuals (r^2 = 0.085) also predicted
large amounts of hornblende fractionation. This seemed
geologically unreasonable for three reasons: (1) the
parent magma (AT5-75) contains only trace amounts of
hornblende, and these crystals typically exhibit
resorption textures in thin section; (2) AT5-75 is the
only thin section examined from the entire Ammonia Tanks
suite that contained hornblende; (3) clinopyroxene
fractionation occurs in steps 2-5 in the regression model,
but not step 1. The fractionation of hornblende before
clinopyroxene seems unlikely. Therefore, clinopyroxene
was substituted for hornblende in step 1 of the major
element regressions. Although the sum of the squares of
the residuals are larger (r^2 = 0.1576) than if hornblende
were used, they are still considerably less than 1.0.
Furthermore, the trace element data (see discussion
below) fit the clinopyroxene fractionation model much
better than the hornblende model.

Feldspar fractionation dominates each step in the
major element regression model. Plagioclase is predicted
to be the major fractionating phase between 59% and 67%
SiO_2 whereas sanidine becomes dominant above 67% SiO_2.
Clinopyroxene, biotite and magnetite make up the balance
of the fractionating phases. The phenocryst compositions
used in each step of the model are give in Table 4.

TABLE 3. MAJOR ELEMENT MULTIPLE LINEAR REGRESSIONS

STEP 1

    PARENT = AT5-75 (59.44% SiO_2)
    DAUGHTER = AT5-63 (62.11% SiO_2)

    AT5-75 = 0.0869 + 0.848 AT5-63 + 0.0923 PLAG + 0.0316 CPX
           + 0.0175 MT

                R^2 = 1.00   SS = 0.1576

STEP 2

    PARENT = AT5-63 (62.11% SiO_2)
    DAUGHTER = AT5-72 (64.00% SiO_2)

    AT5-63 = 0.0890 + 0.896 AT5-72 + 0.0614 PLAG + 0.0212 CPX
           + 0.0096 MT

                R^2 = 1.00   SS = 0.1321

STEP 3

    PARENT = AT5-72 (64.00% SiO_2)
    DAUGHTER = AT5-71 (66.95% SiO_2)

    AT5-72 = -0.0091 + 0.764 AT5-71 + 0.193 PLAG + 0.0285 CPX
           + 0.0161 MT

                R^2 = 1.00   SS = 0.1814

STEP 4

    PARENT = AT5-71 (66.95% SiO_2)
    DAUGHTER = AT5-58 (69.25% SiO_2)

    AT5-71 = 0.0225 + 0.719 AT5-58 + 0.22 KSP + 0.0396 PLAG
           + 0.00888 CPX + 0.00896 MT

                R^2 = 1.00   SS = 0.07865

TABLE 3. (Continued)

STEP 5

PARENT = AT5-58 (69.25% SiO_2)
DAUGHTER = AT5-35 (72.96% SiO_2)

AT5-58 = 0.0547 + 0.672 AT5-35 + 0.294 KSP + 0.0109 PLAG
+ 0.0181 CPX + 0.0144 MT

R^2 = 1.00   SS = 0.004290

STEP 6

PARENT = AT5-35 (72.96% SiO_2)
DAUGHTER = AT5-3 (77.96% SiO_2)

AT5-35 = -0.0067 + 0.696 AT5-3 + 0.0503 PLAG + 0.231 KSP
+ 0.0176 BIOT + 0.00607 MT

R^2 = 1.00   SS = 0.06226

NOTE: These regressions were also calculated with a zero
intercept (see Appendix 4). This removes the B_0
coefficient on the right hand side of the equation
and results in somewhat greater sums of the squares
of the residuals (SS).

TABLE 4.   MINERAL ANALYSES USED IN REGRESSIONS FOR
CRYSTAL FRACTIONATION MODEL

(mineral analyses are from the parent magma)

PLAGIOCLASE

Sample	AT5-75	AT5-63	AT5-72	AT5-71	AT5-58
Step	1	2	3	4	5
Mineral ID	92	38	77	61	15
SiO$_2$	55.17	58.15	58.84	57.77	61.28
Al$_2$O$_3$	28.86	26.26	25.33	26.51	23.70
FeO	0.20	0.32	0.84	0.40	0.38
MgO	0.05	0.01	0.00	0.03	0.00
CaO	9.65	6.67	6.57	6.84	4.68
Na$_2$O	5.25	6.78	6.77	6.94	8.34
K$_2$O	0.54	1.27	1.38	1.01	1.40
BaO	0.18	0.34	0.25	0.39	0.10
TOTALS	99.90	99.80	99.98	99.89	99.88

	PLAGIOCLASE		SANIDINE		
Sample	AT5-35		AT5-71	AT5-58	AT5-35
Step	6		4	5	6
Mineral ID	27		65	14	28
SiO$_2$	63.95		65.21	64.34	65.48
Al$_2$O$_3$	22.59		19.89	20.01	19.29
FeO	0.26		0.24	0.27	0.09
MgO	0.00		0.00	0.00	0.00
CaO	2.77		0.64	0.52	0.38
Na$_2$O	8.71		4.84	5.77	5.16
K$_2$O	1.72		9.17	8.59	9.33
BaO	0.00		0.00	0.38	0.25
TOTALS	100.00		99.99	99.88	99.98

TABLE 4. (Continued)

CLINOPYROXENE

Sample	AT5-75	AT5-63	AT5-72	AT5-71	AT5-58
Step	1	2	3	4	5
Mineral ID	86	35	72	57	12
SiO_2	51.86	52.29	53.52	52.95	52.54
Al_2O_3	2.14	2.13	2.40	2.06	1.17
FeO	7.94	7.52	7.89	7.86	8.26
MgO	15.90	15.49	15.45	15.02	13.64
CaO	20.31	20.76	18.67	20.16	21.94
Na_2O	0.65	0.58	0.59	0.64	0.76
K_2O	0.00	0.01	0.00	0.00	0.00
TiO_2	0.47	0.58	0.52	0.48	0.28
MnO	0.69	0.55	0.93	0.80	1.35
P_2O_5	0.00	0.00	0.00	0.00	0.00
BaO	0.04	0.09	0.03	0.00	0.05
NiO	0.00	0.00	0.00	0.03	0.00
TOTALS	100.00	100.00	100.00	100.00	99.99

MAGNETITE

Sample	AT5-75	AT5-63	AT5-72	AT5-71	AT5-58
Step	1	2	3	4	5
Mineral ID	97	42	83	69	32
Cr_2O_3	0.04	0.00	0.03	0.09	0.03
Al_2O_3	3.61	2.85	2.43	1.47	1.01
MgO	3.25	3.76	2.77	1.66	1.27
FeO	84.20	80.58	81.55	79.54	87.65
TiO_2	8.05	11.81	11.75	15.35	7.75
MnO	0.85	1.01	1.47	1.90	2.29
TOTALS	100.00	100.01	100.00	100.01	100.00

TABLE 4. (Continued)

	BIOTITE			MAGNETITE
Sample	AT5-35		Sample	AT5-35
Step	6		Step	6
Mineral ID	25		Mineral ID	20
SiO_2	40.58		Cr_2O_3	0.02
Al_2O_3	13.67		Al_2O_3	0.82
FeO	15.06		MgO	0.73
MgO	16.56		FeO	90.14
CaO	0.28		TiO_2	6.46
Na_2O	0.58		MnO	1.83
K_2O	8.00			
TiO_2	4.59		TOTAL	100.00
MnO	0.43			
BaO	0.24			
TOTAL	99.99			

NOTE: All analyses have been normalized to 100%

As a second test, these major element regressions were evaluated using trace element data. Ideally, mineral/ liquid distribution coefficients for trace elements used in the model should be calculated for the system of interest. However, this is not always possible because it requires handpicking enough phenocryst and pure glass separates for the chemical analysis of each. Time limitations prevented the determination of distribution coefficients for the Ammonia Tanks. The alternative is to use distribution coefficients that have already been determined for other systems of similar chemistry and inferred P-T conditions. Unfortunately, distribution coefficients often vary significantly from system to system, even for systems of similar chemistry. Therefore every effort was made to examine all of the recent literature that provided compilations of distribution coefficients for intermediate- to high-silica systems to insure that the maximum permissible range in K_D values would be utilized. Distribution coefficient data was compiled (Table 5) from Arth and Hanson (1975), Arth (1976), Henderson (1982), Mahood and Hildreth (1983), Hyndman (1985), and Nash and Crecraft (1985).

The trace elements selected to test the major element regression model are Rb, Sr, Ba, Sc, Ce, Yb and Th. In general, incompatible trace elements exhibiting a wide range in composition, with small measured uncertainties in concentration are best suited for the modeling process.

The availability of distribution coefficient data was the limiting factor in the element selection process. As a result, some of the trace elements used in the model exhibit narrow compositional ranges while others are compatible in one or more mineral phases.

The results of the trace element tests are shown in Table 6. The predicted range of element concentrations are Rayleigh fractionation values. As stated before, for this data to be consistent with the crystal fractionation trends predicted by the major element regressions, the observed trace element concentrations should fall within the fractionation window predicted by the maximum and minimum trace element distribution coefficients.

Some of the lack of agreement between the calculated and observed trace element data shown in Table 6 can be explained by taking into account trace mineral phases that strongly partition certain elements. For instance, the mineral chevkinite, which is present in all samples containing >67% SiO_2, readily accepts the REE's and Th into it's crystal lattice, thereby causing the melt to become depleted in these elements. If chevkinite is excluded from the fractionation model, it would cause the predicted concentrations of Ce, Yb and Th to be higher than they would be if the model included chevkinite. This is precisely what is observed in steps 4, 5, and 6 of the model; the fractionation windows all overpredict the observed element concentrations. By applying the

TABLE 5.   DISTRIBUTION COEFFICIENTS

	PLAGIOCLASE max	PLAGIOCLASE min	SANIDINE max	SANIDINE min	CLINOPYROXENE max	CLINOPYROXENE min
Sc	0.20	0.01	0.059	0.01	172	18
Rb	0.46	0.016	2.4	0.11	0.09	0.032
Sr	33	1.45	26	3.6	0.516	
Ba	3.3	0.3	24	1.0	2.3	0.131
Ce	0.4	0.11	0.095	0.02	21.6	0.36
Yb	0.3	0.049	0.04	0.005	11.6	1.14
Th	0.09	0.01	0.03	0.0095	6.56	0.01

	BIOTITE max	BIOTITE min	MAGNETITE max	MAGNETITE min
Sc	20.0	4.9	15.6	1.5
Rb	5.3	2.24	0	
Sr	0.53	0.12	0	
Ba	36	3.7	0.08	0.05
Ce	11.0	0.037	22.9	0.28
Yb	3.0	0.179	2.2	0.2
Th	2.0	0.27	5.04	0.04

Data compiled from Arth and Hanson (1975), Arth (1976),
Henderson (1982), Mahood and Hildreth (1983),
Hyndman (1985), and Nash and Crecraft (1985).

TABLE 6.   TRACE ELEMENT MODELS

STEP	1	2	3
PARENT	AT5-75	AT5-63	AT5-72
DAUGHTER	AT5-63	AT5-72	AT5-71
Sc predicted	0.02-4.9	0.14-5.0	0.02-4.5
observed	6.9	6.3	6.4
Rb predicted	75-79	80-82	95-104
observed	75 *	80 *	89
Sr predicted	35-811	80-610	0.5-496
observed	615 *	524 *	164 *
Ba predicted	3641-5288	3373-4298	2090-4352
observed	3990 *	3560 *	1168
Ce predicted	75-245	120-247	93-300
observed	228 *	238 *	393
Yb predicted	1.7-2.7	2.0-3.2	2.0-3.2
observed	2.4 *	2.4 *	2.4 *
Th predicted	9.6-13.3	12.6-17.4	12.6-17.4
observed	12.1 *	13.3 *	19.6

*   Indicates good fit

TABLE 6.   (Continued)

STEP	4	5	6
PARENT	AT5-71	AT5-58	AT5-35
DAUGHTER	AT5-58	AT5-35	AT5-3

		4	5	6
Sc	predicted	1.2-7.2	0.1-3.9	1.9-3.0
	observed	3.4 *	2.3 *	1.3
Rb	predicted	65-120	77-177	106-218
	observed	122	164 *	216 *
Sr	predicted	0.06-83	0.01-56	0.01-43
	observed	138	88	7 *
Ba	predicted	2.8-1230	0.2-742	0.3-390
	observed	709 *	394 *	74 *
Ce	predicted	328-534	134-329	120-184
	observed	222.89	129.90	58.48
Yb	predicted	2.8-3.2	3.0-3.9	3.5-3.9
	observed	2.7	2.7	2.9
Th	predicted	23.7-27.0	23.7-30.2	32.0-34.7
	observed	20.1	24.3 *	30.0

* Indicates good fit

Rayleigh fractionation law (see Cox, et al., 1979, p.346)
it was possible to estimate the amount of chevkinite
crystallization needed to bring the predicted element
concentrations into agreement with the observed
concentrations (see appendix 3). It was found that by
fractionating only 0.2% chevkinite, the predicted Ce, Yb
and Th concentrations can all be made to agree with the
observed concentrations of these elements in the melt.
This amount of chevkinite fractionation does not seem
unreasonable based on the observed abundance of
chevkinite in thin section, and it generally accounts
for the discrepancy between the predicted and observed
concentrations of Ce, Yb and Th in steps 4, 5, and 6 of
the model. Fractionation of the minerals apatite and
zircon can be used to account for the chemical variations
exhibited by the elements Zr, Hf and P in a similar
manner.

Several factors other than the fractionation of trace
phases may have also adversely affected the results of
the trace element model. A potentially significant
source of error arises from the fact that the
distribution coefficients used in the trace element tests
were not calculated for the Ammonia Tanks magma system.
As previously discussed, the use of inappropriate
distribution coefficients can result in a lack of
agreement between the predicted and observed trace
element concentrations.

As an example, consider the partitioning of strontium into plagioclase and sanidine. The distribution coefficients used in the model (see Table 5) indicate that Sr is highly compatible in the feldspar minerals. However, in steps 4 and 5 of the trace element model, the predicted range for Sr concentrations is much less than the observed Sr concentrations. There are several possible interpretations for this. It may be that the K_D's correctly predict the the behavior of Sr, and the model simply fails for these steps. Alternatively, it is possible that the distribution coefficients overpredicted the partitioning of Sr into the feldspars. By using smaller distribution coefficients, the predicted and observed concentrations might have concurred. Another potential explanation is that not all of the crystals formed in the parent liquid were actually separated from the residual liquid. In other words, it could be that fewer crystals were separated from the liquid than was predicted by the major element regression.

Analytical error is another factor that may have affected the results of the model. Trace elements that are present in low concentrations, or those that exhibit narrow compositional ranges may exhibit discrepancies between the predicted and observed concentrations due to analytical error. This problem will be compounded by the use of inappropriate distribution coefficients. Of the elements used in the trace element model, Sc and Yb would

be the most susceptible to this type of error because
they are present in concentrations that are near the
detectibility limit.

Finally, an important factor that must be considered
is the possibility that other magma differentiation
processes acted in conjunction with fractional
crystallization. Several independent lines of evidence
indicated that magma mixing may have taken place between
the time of eruption of the Rainier Mesa Member and the
Ammonia Tanks Member. Since magma mixing can easily be
evaluated, it is logical that the possibility of magma
mixing in the Ammonia Tanks system should be explored
before drawing any conclusions based exclusively on the
crystal fractionation model.

EVALUATION OF MAGMA MIXING

The potential for generating compositional variations
due to magma mixing has been demonstrated for a number of
silicic systems (cf. Reid, et al., 1983; Vogel, et al.,
1984). In ash flow sheets, the presence of disequilibrium
phenocryst populations within individual pumice fragments
is a strong indication that magma mixing may have occurred
(Vogel, et al., 1987). Disequilibrium phenocryst textures
were observed to some extent in all thin sections of
Ammonia Tanks pumice fragments. These textures are
strongly developed among the low-silica pumice fragments,
particularly in samples that contain between 59% and 69%

SiO_2 .

Plagioclase grains exhibit the most pronounced disequilibrium textures at all silica compositions. In pumice fragments containing <69% SiO_2, many plagioclase grains are deeply embayed, and sieve-like textures are widely developed. Resorption textures are also common in clinopyroxene grains. Biotite and the opaque Fe-Ti oxides appear to be affected far less than the feldspars and pyroxene. In pumice fragments containing >69% SiO_2, only the feldspars exhibit disequilibrium textures, primarily in the form of minor embayments along grain boundaries. Not surprisingly, microprobe analyses show that the feldspar and clinopyroxene grains exhibit the greatest compositional heterogeneities among phenocrysts within any given glassy pumice fragment.

It is notable that banded pumice were sometimes found in the Ammonia Tanks Member, particularly in the stratigraphic horizons where mafic pumice were predominant. Most of these banded pumice were composed of phenocryst-rich orangish-brown glass that was streaked with phenocryst-poor white glass. While this is not prima facie evidience of magma mixing, it does indicate some commingling of heterogeneous magmas. However, it is uncertain if the commingling occured in the magma chamber, or during eruption.

As previously discussed, apparent gaps are observed in the silica composition of the Ammonia Tanks ash-flow sheet.

These gaps occur between 67% and 69% SiO_2, between 70.7% and 73% SiO_2, and again between 73.8% and 76.8% SiO_2, possibly indicating the presence of sharp compositional interfaces between magma bodies of contrasting composition. It was hypothesized that the magma represented by intermediate SiO_2 compositions may have formed from mixing of the high-silica rhyolite (>76% SiO_2) and low-silica quartz latite (<67% SiO_2) magmas. Magma mixing can be readily evaluated using element-element and ratio-ratio plots (Langmuir, et al., 1977). Data points representing mixed magmas should plot along a straight line on x-y element-element plots, and along a hyperbolic curve on x-y plots of element ratios (A/B v.s. C/D).

A number of element-element plots were made using various trace elements, but strictly linear trends were rarely seen. Ratio-ratio plots of incompatible elements also failed to produce the hyperbolic curve expected if magma mixing had been the dominant magma differentiation process. However these tests did not preclude the possibility that magma mixing acted in conjunction with crystal fractionation.

Magma mixing plus crystal fractionation can be evaluated using major element multiple linear regressions in much the same way as crystal fractionation alone is evaluated. The only difference is that the regression equation is now set up so that the hybrid magma is equal to the sum of the two mixed magmas minus the fractionated

phenocryst phases. Several different pumice fragments of intermediate silica composition were tested as potential candidates for a mixed + fractionated magma. The best result obtained was:

$$AT5\text{-}35 = -0.0442 + 0.539\ AT5\text{-}71 + 0.513\ AT5\text{-}3 - 0.0372\ KSP$$
$$-0.00754\ PLAG - 0.00266\ CPX$$

$$SS = 0.04616 \qquad R^2 = 1.00$$

If the regression equation is restricted to mixing of end-member compositions (i.e. the most primitive and most evolved pumice fragment compositions) then the best result was:

$$AT5\text{-}35 = 0.022 + 0.501\ AT5\text{-}75 + 0.704\ AT5\text{-}3 - 0.0584\ CPX$$
$$-0.135\ PLAG - 0.014\ MT$$

$$SS = 0.2469 \qquad R^2 = 1.00$$

These regressions were also calculated with a zero intercept for comparative purposes (results are given in Appendix 4). Phenocryst compositions used in these models are given in Table 7. These results are consistent with the interpretation that crystal fractionation along with magma mixing can explain the chemical and mineralogical trends observed in the Ammonia Tanks ash-flow sheet.

TABLE 7.   MINERAL ANALYSES USED IN REGRESSIONS FOR
              CRYSTAL FRACTIONATION + MAGMA MIXING MODEL
           (mineral analyses are from the derivitive magma)

A. Derivitive magma = AT5-35 (72.96% SiO_2)

    Mixed magmas = AT5-71 (66.95% SiO_2)
                   AT5-3 (77.96% SiO_2)

	PLAGIOCLASE	SANIDINE	CLINOPYROXENE
Mineral ID	27	28	22
SiO_2	63.95	65.48	52.75
Al_2O_3	22.59	19.29	0.81
FeO	0.26	0.09	9.01
MgO	0.00	0.00	13.23
CaO	2.77	0.38	21.43
Na_2O	8.71	5.16	0.67
K_2O	1.72	9.33	0.02
BaO	0.00	0.25	0.09
TiO_2			0.20
MnO			1.76
NiO			0.04
TOTALS	100.00	99.98	100.01

B. Derivitive magma = AT5-35

    Mixed magmas = AT5-75 (59.44% SiO_2)
                   AT5-3 (77.96% SiO_2)

    Note: The plagioclase composition used in this model
           is the same as the composition given above.

CLINOPYROXENE		MAGNETITE	
Mineral ID	23	Mineral ID	20
SiO_2	52.50	Cr_2O_3	0.02
Al_2O_3	0.93	Al_2O_3	0.82
FeO	7.74	MgO	0.71
MgO	14.96	FeO	90.14
CaO	22.52	TiO_2	6.46
Na_2O	0.45	MnO	1.83
K_2O	0.00		
BaO	0.00	TOTAL	99.98
TiO_2	0.20		
MnO	0.70		
NiO	0.00		
TOTAL	100.00		

DISCUSSION AND CONCLUSIONS

This study was aimed at determining whether the most
evolved high-silica rhyolite present in the Ammonia Tanks
Member of the Timber Mountain Tuff can be modeled as
originating from the quartz latitic magma by fractional
crystallization. The results of a series of six major
element multiple linear regressions strongly supports the
proposed model. The regressions predicted plagioclase
and magnetite fractionation throughout the compositional
evolution of the magma. Clinopyroxene fractionation was
predicted for the first five steps in the model (up to 73%
SiO_2), after which biotite fractionation was predicted.
Sanidine fractionation was important in the last three
steps of the model (above 67% SiO_2). These predictions
seem geologically reasonable based on petrographic
analyses of the samples used in the model.

Evaluation of the major element multiple linear
regressions using trace element data produced largely
favorable results (Table 6). Much of the lack of
agreement between the predicted and observed trace element
concentrations can be accounted for by the fractionation
of mineral phases that were not included in the regression
model. As previously discussed, fractionation of the
mineral chevkinite can account for discrepancies between
the predicted and observed concentrations of Ce, Yb and
Th in steps 4, 5 and 6. Similarly, zircon and sanidine
fractionation can account for inconsistencies in Th and

57

Ba concentrations, respectively, in step 3.

The use of inappropriate distribution coefficients can also result in a lack of agreement between predicted and observed trace element concentrations. For example, the model can overpredict the partitioning of an element into certain mineral phases if the distribution coefficients used are too large. This may have been the case for Sc partitioning in clinopyroxene and magnetite (steps 1, 2 and 3) and Sr partitioning in plagioclase and sanidine (steps 4 and 5).

Discordant predicted and observed Rb concentrations (steps 3 and 4) may be due to the fact that Rb, like Na and K, is highly susceptible to remobilization due to the secondary hydration of pumice fragments. Rb is also strongly partitioned by biotite. Although biotite was observed to be present in all Ammonia Tanks samples examined, it was not included in the first five steps of the major element multiple linear regression model because it did not improve the statistical results. Thus, the fractionation of small amounts of biotite in these steps might also account for the discrepancy in Rb concentration.

The presence of disequilibrium phenocrysts is not explained by the crystal fractionation model. Therefore, the possibility that the high-silica rhyolite and quartz latite magmas mixed to form a magma of intermediate composition was tested. Major element multiple linear

regression tests demonstrated that Ammonia Tanks magma of
rhyolitic composition (73% SiO_2) can originate from a
combination of magma mixing and crystal fractionation.
The best fit mixing + fractionation regression model
predicts the mixing of subequal proportions of quartz
latite (AT5-71) and high-silica rhyolite (AT5-3) and the
fractionation of 3.4% sanidine and <1% plagioclase and
clinopyroxene. Modal phenocryst abundances in the
derivitive magma (AT5-35) are roughly proportional to the
quantities expected based on the calculated percentages
of mixing and fractionation.

Magma mixing most likely occurred due to the disruption
of compositional zonations in the magma chamber resulting
from the eruption of the Rainier Mesa Member of the Timber
Mountain Tuff. Quartz latite and high-silica rhyolite
pumice fragments of similar composition to those used in
the mixing + fractionation model occur together at the top
of the Rainier Mesa ash-flow sheet (Mills and Rose, 1986).
This indicates that neither of these magma types were
completely evacuated during the eruption of the Rainier
Mesa Member. Therefore, it is inferred that the
turbulence brought about by the Rainier Mesa eruption
resulted in the mixing of at least some of the unerupted
volumes of high-silica rhyolite and quartz latite to form
a rhyolitic magma.

Although these results demonstrate that magma mixing
can act in conjunction with crystal fractionation to

produce the observed compositional trends, this does not prove that there is any correlation between the observed compositional gaps in silica and the mixing event. Changes in slope on some trace element plots v.s. SiO_2 can be correlated with some of the silica gaps; while many of these inflections can be attributed to crystal fractionation, there are notable exceptions. For instance, there is no ready explanation for the change in slope that occurs at 75% SiO_2 on plots of highly incompatible elements (Rb, Nb, Th) v.s. SiO_2 (see Figure 5). If these inflections are related to the proposed mixing event, then it may be that they are observed on incompatible element plots simply because of the minimal effect that crystal fractionation has on these elements.

A larger data base could be used to determine if the observed silica gaps really exist, or if they are an artifact of sampling bias. However, it seems likely that the observed inflections in chemical trends must ultimately be related to some magma differentiation process. Based on the results of this study, it appears that a combination of crystal fractionation with subordinate magma mixing provides a plausible explanation for these trends that is consistent with the data.

To summarize, it has been demonstrated that the high-silica rhyolite of the Ammonia Tanks Member of

the Timber Mountain Tuff can be modeled as originating
from the quartz latite as a result of fractional
crystallization. However, to explain the presence of
pervasive disequilibrium phenocrysts in these rocks,
it was necessary to include an additional magma
differentiation process in the model. Magma mixing
was combined with crystal fractionation to give a
model that is consistent with both the chemical data
and the textural observations. Crystal fractionation
is favored as the dominant magma differentiation
mechanism because it can be used to model the chemical
evolution of the Ammonia Tanks magma system by itself
whereas magma mixing cannot.

APPENDICES

APPENDIX 1

SAMPLE LOCATIONS

Samples	Location
AT4-14 to AT4-75	NE 1/4, SE 1/4, S 1/2, Silent Butte 7.5 Min. Quad. Approximately 0.7 km north of Pahute Mesa Rd., near South Silent Canyon
AT5-2 to AT5-79	SE 1/4, SE 1/4, S 1/2, Silent Butte 7.5 Min. Quad. 1 km southeast of Pahute Mesa Exploratory Hole 1 along Pahute Mesa Rd.

APPENDIX 2

SAMPLE PREPARATION TECHNIQUES

A. To leach secondary carbonate minerals from pumice
    samples.

    For each sample, prepare the following solution:

    (1) measure 41 g. of sodium acetate
    (2) add 13.5 ml. of glacial acetic acid
    (3) add enough distilled water to make 500 ml.

    The sample should be crushed to no larger than pea-

    sized fragments. Add the crushed sample to the

    solution and and boil for 30 minutes, stirring

    occasionally. Allow to settle, then flush four

    times with distilled water, centrifuging between

    rinses.

B. To prepare glass wafers for XRF analysis

    Combine the following in a Pt-Au alloy crucible:

    (1) 9.0000 g. lithium tetraborate
    (2) 1.0000 g. finely crushed and leached sample
    (3) 0.160 g. ammonium nitrate

    Carefully homogenize the contents of the crucible.

    Heat this mixture to ~1100°C with a bunsen burner

    for 30 minutes while gently shaking the crucible.

    A homogeneous molten liquid should result. Pour

    the liquid into a hot Pt-Au alloy mold and allow to

    cool on a hot plate.

APPENDIX 3

A METHOD FOR THE DETERMINATION OF TRACE PHASE
FRACTIONATION PERCENTAGES

The Rayleigh fractionation law is given by Cox, et al.,

(1979) as

$$C_L/C_o = F^{(D-1)} \qquad (1)$$

where C_L = conc. of element in derivitive liquid
C_o = initial concentration of element in the
parent magma
F = proportion of original liquid remaining
D = bulk dist coeff = $\sum w_i K_{Di}$
w_i = the wt. % of the ith mineral phase
K_{Di} = the mineral/liquid partition coefficient
for an element in the ith mineral phase

Taking logs of both sides of equation (1) and rearranging

gives the expression

$$\log F + \log (C_L/C_o) = D \log F \qquad (2)$$

which can be solved for D if F, C_L and C_o are given.

As an example of how to determine the percentage of

chevkinite fractionation needed to bring the predicted and

observed trace element concentrations into agreement,

consider the partitioning of Ce in step 4 of the

fractionation model. The observed Ce concentrations are:

C_L = 222.89 ppm Ce (in AT5-58)
C_o = 393.42 ppm Ce (in AT5-71)

The amount of crystallizaion predicted by the major element

regression in step 4 was 27.74%. Therefore,

$$F = 1.00 - 0.2774 = 0.7226$$

Using equation 2, D is readily determined to be 2.749.

Although K_D values were not available for chevkinite,
Mahood and Hildreth (1983) give K_D's for Ce, Yb and Th in
the mineral allanite (K_D for Ce in allanite = 2063 $\pm$ 30).
Allanite and chevkinite are similar enough in structure
that we can assume they will partition the REE's and Th in
a similar manner. This allows for reasonable estimates of
the degree of chevkinite fractionation. For step 4,
we can write

D = (wt % sanidine)(K_D Ce in sanidine) + (wt % plag) x
   (K_D Ce in plag) + (wt % cpx)(K_D Ce in cpx) +
   (wt % magnetite)(K_D Ce in magnetite) +
   (wt % chevkinite)(K_D Ce in Chevkinite)

The wt %'s of fractionation mineral phases (predicted by
the major element regression) are normalized to 100%.
Letting x = the amount of chevkinite fractionation, and
plugging in appropriate K_D's gives the following
expression

D = 2.749 = (0.793-x)(0.02) + (0.1427-x)(0.11) +
    (0.032-x)(0.36) + (0.0323-x)(0.28) + 2063x.

Solving for x gives 1.308×10^{-3}, or 0.13% chevkinite
fractionation. Similar calculations were carried out for
Yb and Th. The maximum amount of chevkinite fractionation
predicted by this method for steps 4, 5 and 6 was 0.21%.

APPENDIX 4

MAJOR ELEMENT MULTIPLE LINEAR REGRESSIONS CALCULATED WITH Y-INTERCEPTS EQUAL TO ZERO

A. CRYSTAL FRACTIONATION MODEL

STEP 1

    PARENT = AT5-75 (59.44% SiO_2)
    DAUGHTER = AT5-63 (62.11% SiO_2)

    AT5-75 = 0.844 AT5-63 + 0.0963 PLAG + 0.0338 CPX
            + 0.0186 MT

                R^2 = 1.00   SS = 0.1943

STEP 2

    PARENT = AT5-63 (62.11% SiO_2)
    DAUGHTER = AT5-72 (64.00% SiO_2)

    AT5-63 = 0.890 AT5-72 + 0.0677 PLAG + 0.0236 CPX
            + 0.0109 MT

                R^2 = 1.00   SS = 0.1718

STEP 3

    PARENT = AT5-72 (64.00% SiO_2)
    DAUGHTER = AT5-71 (66.95% SiO_2)

    AT5-72 = 0.765 AT5-71 + 0.192 PLAG + 0.0238 CPX
            + 0.0160 MT

                R^2 = 1.00   SS = 0.1942

STEP 4

    PARENT = AT5-71 (66.95% SiO_2)
    DAUGHTER = AT5-58 (69.25% SiO_2)

    AT5-71 = 0.711 AT5-58 + 0.229 KSP + 0.0393 PLAG
            + 0.0103 CPX + 0.00928 MT

                R^2 = 1.00   SS = 0.08818

STEP 5

    PARENT = AT5-58 (69.25% SiO_2)
    DAUGHTER = AT5-35 (72.96% SiO_2)

    AT5-58 = 0.634 AT5-35 + 0.340 KSP + 0.0019 PLAG
           + 0.0187 CPX + 0.00502 MT

           R^2 = 1.00   SS = 0.1000

STEP 6

    PARENT = AT5-35 (72.96% SiO_2)
    DAUGHTER = AT5-3 (77.96% SiO_2)

    AT5-35 = 0.697 AT5-3 + 0.230 KSP + 0.0501 PLAG
           + 0.0172 BIOT + 0.00606 MT

           R^2 = 1.00   SS = 0.06764

B. CRYSTAL FRACTIONATION + MAGMA MIXING MODEL

1. Best fit model (overall)

    DERIVITIVE MAGMA = AT5-35 (72.96% SiO_2)
    MIXED MAGMAS = AT5-71 (66.95% SiO_2)
              AT5-3 (77.96% SiO_2)

    AT5-35 = 0.519 AT5-71 + 0.525 AT5-3 - 0.00442 PLAG
           - 0.0338 KSP - 0.00452 CPX

           R^2 = 1.00   SS = 0.05489

2. Mixing of end-member compositions

    DERIVITIVE MAGMA = AT5-35 (72.96% SiO_2)
    MIXED MAGMAS = AT5-75 (59.44% SiO_2)
              AT5-3 (77.96% SiO_2)

    AT5-35 = 0.508 AT5-75 + 0.702 AT5-3 - 0.138 PLAG
           - 0.0583 CPX - 0.0140 MT

           R^2 = 1.00   SS = 0.2479

LIST OF REFERENCES

LIST OF REFERENCES

Aramaki, S., and Lipman, P.W., 1965. Possible leaching of
    Na_2O during hydration of volcanic glasses. Japan Acad.
    Proc., 41: 467-470.

Arth, J.G., 1976. Behavior of trace elements during
    magmatic processes: A summary of theoretical models and
    their applications. Jour. Research U.S. Geol. Surv., 4:
    41-47.

Arth, J.G., and Hanson, G.N., 1975. Geochemistry and
    origin of the early Precambrian crust of northeastern
    Minnesota. Geochem. Cosmochim. Acta, 39: 325-362.

Baker, B.H. and McBirney, A.R., 1985. Liquid Fractionation.
    Part III: Geochemistry of zoned magmas and the
    compositional effects of liquid fractionation.
    J. Volcanol. Geotherm. Res., 24: 55-81.

Blake, S., 1981. Eruptions from zoned magma chambers.
    J. Geol. Soc. London, 138: 281-287.

Blake, S. and Ivey, G.N., 1986. Magma-mixing and the
    dynamics of withdrawal from stratified reservoirs.
    J. Volcanol. Geotherm. Res., 27: 153-178.

Bowen, N.L., 1928. The Evolution of the Igneous Rocks.
    Princeton University Press: 334 p.

Broxton, D.E., Byers, F.M., Jr., Warren, R.G., and Scott,
    R., 1985. Trends in phenocryst chemistry in the Timber
    Mountain-Oasis Valley volcanic field, SW Nevada:
    Evidence for episodic injection of primitive magma into
    an evolving magma system (abstract). Geol. Soc. Am.
    Abstr. Programs, 17: 345.

Byers, F.M., Jr., Carr, W.J., Christiansen, R.L., Lipman,
    P.W., Orkild, P.P. and Quinlivan, W.D., 1976a. Geologic
    map of the Timber Mountain caldera area, Nye County,
    Nevada: U.S. Geol. Surv. Miscellaneous Geologic
    Investigations Map I-891.

Byers, F.M., Jr., Carr, W.J., Orkild, P.P., Quinlivan, W.D. and Sargent, K.A., 1976b. Volcanic suites and related cauldrons of Timber Mountain-Oasis Valley caldera complex, southern Nevada. U.S. Geological Survey Professional Paper 919, 70p.

Cameron, K.L., 1983. Bishop Tuff revisited: New rare-earth element data consistent with crystal fractionation. Science, 224: 1338-1340.

Carr, W.J., Byers, F.M., Jr., and Orkild, P.P., 1984. Stratigraphic and volcano-tectonic relations of Crater Flat Tuff and some older volcanic units, Nye County, Nevada. U.S. Geol. Surv. Open-File report 84-114: 42 pp.

Christiansen, R.L. and Lipman, P.W., 1972. Cenozoic volcanism and plate-tectonic evolution of the Western United States. II. Late Cenozoic: Phil. Trans. R. Soc. London, A 271: 249-284.

Christiansen, R.L., Lipman, P.W., Carr, W.J., Byers, F.M., Jr., Orkild, P.P. and Sargent, K.A., 1977. Timber Mountain-Oasis Valley caldera complex of southern Nevada. Geol. Soc. Am. Bull., 88: 943-959.

Cox, K.G., Bell, J.D. and Pankhurst, R.J., 1979. The Interpretation of Igneous Rocks. George, Allen and Unwin, London: 450 p.

Deer, W.A., Howie, R.A., and Zussman, J., 1962. Rock-Forming Minerals, v.1, Ortho- and Ring Silicates. Longmans, Green and Co., London: 333p.

Ekrin, E.B., Anderson, R.E., Orkild, P.P., and Hinrichs, E.N., 1966. Geology of Silent Butte quadrangle, Nye County, Nevada: U.S. Geol. Survey Geol. Quad. Map GQ-493.

Flood, T.P., 1987. Cyclic evolution of a magmatic system: The Paintbrush Tuff, SW Nevada volcanic field [Ph.D. thesis]. Michigan State University, 147 p.

Hagan, R.C., 1982. X-ray fluorescence analysis: Major elements in silicate minerals. Los Alamos-9400-MS: 1-13.

Haskin, L.A., Haskin, M.A., Frey, F.A., and Wildeman, T.R., 1968. Relative and absolute terrestrial abundances of the rare earths, in Origin and distribution of the elements, L.H. Ahrens, Ed., Pergamon Press, New York: 889-912.

Henderson, P., 1982. Inorganic Geochemistry. Pergamon Press, Oxford: 353p.

Hildreth, E.W., 1977. The magma chamber of the Bishop Tuff: Gradients in temperature, pressure and composition [Ph.D. thesis]. Berkeley, University of California, 328 p.

Hildreth, E.W., 1979. The Bishop Tuff: Evidence for the origin of compositional zonation in silicic magma chambers. Geol. Soc. Am. Special Paper 180, pp. 43-75.

Hildreth, E.W., 1981. Gradients in silicic magma chambers: Implications for lithospheric magmatism. J. Geophys. Res., 86: 10153-10192.

Hyndman, D.W., 1985. Petrology of igneous and metamorphic rocks, 2nd ed., McGraw Hill, New York: 786p.

Kistler, R.W., 1968. Potassium-argon ages of volcanic rocks in Nye and Esmeralda Counties, Nevada, in Nevada Test Site: Geol. Soc. Am. Mem. 110, p. 251-262.

Langmuir, C.H., Vocke, R.D., Hanson, G.N., and Hart, S.R., 1977. A general mixing equation: applied to the petrogenesis of basalts from Iceland and Reykjanes Ridge. Earth Planet. Sci. Lett., 37: 380-392.

Lipman, P.W., 1965. Chemical comparison of glassy and crystalline volcanic rocks. Geol. Soc. Am. Special Paper 82: 260-261.

Lipman, P.W., 1971. Iron-titanium oxide phenocrysts in compositionally zoned ash-flow sheets from southern Nevada. J. Geol., 79: 438-456.

Lipman, P.W., Christiansen, R.L. and O'Conner, J.T., 1966. A compositionally zoned ash-flow sheet in southern Nevada. U.S. Geol. Surv. Prof. Paper 524-F: 47 pp.

Mahood, G.A., 1981. A summary of the geology and petrology of the Sierra La Primavera, Jalisco, Mexico. Jour. Geophys. Res., 86, No. B11: 10137-10152.

Mahood, G.A., and Hildreth, E.W., 1983. Large partition coefficients for trace elements in high-silica rhyolites. Geochem. Cosmochim. Acta, 47: 11-30.

Marvin, R.F., Byers, F.M., Jr., Mehnert, H.H., Orkild, P.P. and Stern, T.W., 1970. Radiometric ages and stratigraphic sequence of volcanic and plutonic rocks, southern Nye and western Lincoln Counties, Nevada. Geol. Soc. Am. Bull., 81: 2657-2676.

Michael, P.J., 1983. Chemical differentiation of the Bishop Tuff and other high-silica magmas through crystallization processes. Geology, 11: 31-34.

Miller, C.F. and Middlefehldt, D.W., 1984. Extreme fractionation in felsic magma chambers: a product of liquid-state diffusion or fractional crystallization? Earth Planet. Sci. Lett., 68: 151-158.

Mills, J.G., Jr., and Rose, T.P., 1986. Geochemistry of glassy pumices from the Timber Mountain Tuff, Southwestern Nevada (abstract). EOS, Trans., AGU, 67: 1262.

Nash, W.P., and Crecraft, H.R., 1985. Partition coefficients for trace elements in silicic magmas. Geochem. Cosmochim. Acta, 49: 2309-2322.

Noble, D.C., 1965. Ground-water leaching of sodium from quickly cooled volcanic rocks (abstract). Am. Mineral., 50: 289.

Noble, D.C., 1967. Sodium, potassium, and ferrous iron contents of some secondarily hydrated natural silicic glasses. Am. Mineral., 52: 280-286.

Noble, D.C., Krushensky, R.D., McKay, E.J., and Ege, J.R., 1967. Geologic map of the Dead Horse Flat quadrangle, Nye County, Nevada: U.S. Geol. Survey Geol. Quad. Map GQ-614.

Noble, D.C., Vogel, T.A., Weiss, S.I., Erwin, J.W., McKee, E.H., and Younker, L.W., 1984. Stratigraphic relations and source areas of ash-flow sheets of the Black Mountain and Stonewall Mountain Volcanic Centers, Nevada. J. Geophys. Res., 89: 8593-8602.

Reid, J.B., Evans, O.C., and Fates, D.G., 1983. Magma mixing in granitic rocks of the central Sierra Nevada, California. Earth Planet. Sci. Lett., 66: 243-261.

Schuraytz, B.C., Vogel, T.A. and Younker, L.W., 1983. Pumice heterogeneity in the Topopah Spring Member of the Paintbrush Tuff: Implications for ash-flow eruption dynamics (abstract). EOS, Trans., AGU, 64: 896.

Schuraytz, B.C., Vogel, T.A. and Younker, L.W., 1986. Geochemical gradients in the Topopah Spring Member of the Paintbrush Tuff: Evidence for eruption across a magmatic interface. Lawrence Livermore National Laboratory report UCRL-53698: 59 pp.

Smith, R.L., 1960. Ash Flows. Geol. Soc. Am. Bull., 71: 795-842.

Smith, R.L., 1979. Ash-flow magmatism. Geol. Soc. Am. Special Paper 180: 5-27.

Smith, R.L., and Bailey, R.A., 1966. The Bandelier Tuff - A study of ash-flow eruption cycles from zonal magma chambers. Bull. Volcanol., 29: 83-103.

Spera, F.J., 1984. Some numerical experiments on the withdrawal magma from crustal reservoirs. J. Geophys. Res., 89: 8222-8236.

Vogel, T.A., Younker, L.W., Wilband, J.T., and Kampmueller, E., 1984. Magma mixing: the Marsco Suite, Isle of Skye, Scotland. Contrib. Mineral. Petrol., 79: 411-423.

Vogel, T.A., Ryerson, F.J., Noble, D.C., and Younker, L.W., 1987. Limits to magma mixing based on chemistry and mineralogy of pumice fragments erupted from a chemically zoned magma body. J. Geol., 95: 659-670.

Williams, H., 1941. Calderas and their origin. University of California, Publications in Geological Sciences, 25: 239-346.

Wolff, J.A., and Storey, M., 1984. Zoning in highly alkaline magma bodies. Geological Magazine, 121: 563-575.

Wright, T.L., 1974. Presentation and interpretation of chemical data for igneous rocks. Contrib. Mineral. Petrol. 48: 233-248.